Synthesis of green thermo-responsive amphoteric terpolymer functionalized silica nanocomposite derived from waste vegetable oil triglycerides for enhanced oil recovery (EOR)

Shahenda Mahran[1, 2*], Attia Attia[2], Basudeb Saha[3*]

[1]School of Engineering, London South Bank University, 103 Borough Road, London, SE1 0AA, UK.
[2]Faculty of Energy and Environmental Engineering, The British University in Egypt, Misr-Ismailia Road, El-Sherouk City 11837, Cairo, Egypt.
[3]School of Engineering, Lancaster University, Lancaster, LA1 4YR, UK.

*Corresponding author(s):
E-mail addresses: b.saha@lancaster.ac.uk (B. Saha); mahrans@lsbu.ac.uk (S. Mahran)

Abstract

Despite the high efficiency of polymer flooding as a chemical enhanced oil recovery (CEOR) technique, the low thermal stability and poor salt resistance of widely applied partially hydrolyzed polyacrylamide (HPAM) limited the application of this technique in oil reservoirs at harsh reservoir conditions of high–temperature and high–salinity (HTHS). These inadequacies of HPAM, result in the urge for an environmentally friendly polymer with good viscosifying properties and a substantial effect on mobility ratio at HTHS reservoir conditions. In this research, a high oleic acid waste vegetable oil (WVO) is utilized to synthesize a novel environmentally benign, thermo-responsive amphoteric nanocomposite for EOR applications at HTHS reservoir conditions. A green route transesterification reaction has been utilized to synthesize a novel thermo-sensitive monomer from WVO. The existence of unsaturated fatty acids isolated double bonds and acryloyl functional groups in the synthesized monomer has been confirmed using different characterization methods. The reactive acryloyl double bond in the synthesized monomer has been copolymerized with acrylamide, acrylacyloxyethyltrimethyl ammonium chloride, and 2-acrylamide-2-methylpropane sulfonic acid in presence of dimethylphenylvinylsilane *via* free radical emulsion polymerization. The synthesized nanocomposite has been characterized by FTIR, ^{1}H NMR, SEM, EDX, TEM, and DLS. The thermal stability of the nanocomposite has been evaluated by TGA and DTA analysis. The results indicated that nanocomposite solution exhibited a pouncing thermo-thickening behaviour and superior viscosifying properties even at an ultra-low polymer concentration of 0.04 wt.% as the temperature increased from 25 to 100 ˚C, with increasing salinity from 10,000 to 230,000 ppm as well as salt-free solutions. Flooding experiments demonstrated that the oil recovery factor reached 15.4±0.1 % using low nanocomposite concentrations of 0.04 wt.%, 22.6±0.3 % using nanocomposite concentrations of 0.06 wt.% and 25±0.2 % using 0.1 wt.% nanocomposite concentrations evaluated under hostile conditions of 100 ºC and salinity of about 230,000 ppm. This research offers a new direction for the synthesis of a novel green, high molecular weight thermo-responsive nanocomposite for EOR application at extremely harsh reservoir conditions *via* WVO valorization.

Keywords

Thermo-responsive terpolymer; Free radical polymerization; Polymer nanocomposite; Waste vegetable oil valorization; Enhanced oil recovery.

1. Introduction

Waste vegetable oils (WVOs) are one of the most abundant sustainable sources and essential raw materials for the synthesis of green valuable chemicals (Gunstone, 2012; Aboelazayem et al., 2021; Umar et al., 2022). Recently published literature has reported different attempts regarding the utilization of edible oil as a renewable platform for the synthesis of valuable biopolymers, composites, and resins such as acrylated resins and epoxy for different industrial applications (Adekunle et al., 2010; Fernandes et al., 2019; Machado et al., 2017). However, the negative effect of the consumption of food recourses and feed chain limited the commercial use of edible oil in the synthesis of biopolymers and composites (Suzuki et al., 2018). The application of WVO in polymer synthesis offers an opportunity to produce biopolymers and composites by waste valorization. Although vegetable oil-derived monomers and polymeric materials were recently investigated for different applications i.e. coating, water treatment, and biosurfactant manufacture, few studies were reported on their potential for EOR applications.

In petroleum reservoirs, only 30 % of the original oil in place (OOIP) can be produced by conventional oil recovery techniques leaving behind approximately 70 % of OOIP in the reservoir. The British Petroleum (BP) Statistic Review of World Energy has stated that around 2,000 billion barrels of crude oil is unrecoverable (Dudley, 2018). Chemically enhanced oil recovery (CEOR) processes, which involve polymer flooding target the amount of hydrocarbon that cannot be recovered using conventional oil recovery methods. Polymer flooding aims at increasing the viscosity of the displacing fluid which enhances sweeping efficiency and reduces the amount of residual oil (Liu et al., 2018; Sayyouh et al., 1993). Since 1990, polymer flooding has been extensively applied in China petroleum companies, and most extracted oilfields at low/medium salinity and reservoir temperatures less than 60 ˚C (Kamal et al., 2015a). More attention has been attracted to oil reservoirs at high–temperatures and high–salinity (HTHS) such as Tarim Oilfield where the water salinity is higher than 110,000 ppm, reservoir temperature is around 100 ˚C, and OOIP up to 300 million tons. However, the low salt tolerance and poor thermal stability of used polymers mostly partially hydrolyzed polyacrylamide (HPAM), hindered polymer flooding application under harsh conditions.

HPAM is the most applied polymer in CEOR with a high viscosifying behaviour in fresh water and low temperature, due to its high molecular weight and capability to form 3D-network structures in an aqueous solution *via* van der Waals forces (Zhang et al., 2014; Mahran et al., 2018). In the presence of salt, their solutions display a significant decrease in viscosity (El-Hoshoudy et al., 2018; Mahran et al., 2018). This behaviour is interpreted by the charge shielding effect, which results in reducing the electrostatic repulsion and subsequently lowering the expansion of the polymer chains (Akbari et al., 2019). This results in a diminution in the hydrodynamic volume and lower viscosity (Kamal et al., 2015a). HPAM also exhibits chain degradation and thermal hydrolysis at severe salinity and temperature. Polymer flooding EOR technique is crucial nowadays, however, HPAM cannot adapt to oil reservoirs at HTHS reservoir conditions due to the degradation of their chains and poor mechanical stability (Lai et al., 2016; Tian et al., 2014).

Accordingly, to overcome the limitations of HPAM, Hourdet and his coworkers (Hourdet et al., 1994; Petit et al., 2007; L'alloret et al., 1997) introduced the concept of "thermo-thickening" or "thermoviscofying" polymers (TVP's). These polymers are characterized by the presence of thermo-sensitive "grafts" that have the property of lower critical solution temperature (LCST) and are attached to the hydrophilic backbone polymer structure (Kamal et al., 2015b). The resulting thermoviscofying polymer has a high solubility at room temperature; however, thermo-sensitive blocks tend to form hydrophobic aggregations with increasing temperature to a critical association temperature (T_{cass}). The formed aggregations of LCST side chains and physical network structure result in an increment of the solution viscosity with any further increase in temperature (Kamal et al., 2015b).

The literature reported two categories of thermo-sensitive functionalities which are incorporated into polymer hydrophilic backbone *via* grafting method: first, polyethylene oxide (PEO)/ polyethylene copolymers and poly(propylene oxide) (PPO) which are introduced onto a hydrophilic polymer *via* a coupling reaction (L'alloret et al., 1995; Bastiat et al., 2002; Wang et al., 2010), second, N-isopropylacrylamide (NIPAM)- amino end macromonomer (Durand and Hourdet, 1999) or NIPAM copolymers (Durand and Hourdet, 2000). These TVP polymers applied in HTHS oil reservoirs will not overcome the limitations of HPAM due to their low viscosity. However, the unique mechanism of these polymers in increasing the viscosity of aqueous solutions makes these polymers more efficient than other polymers utilized for the same purpose. The synthesis of TVP polymers using PEO and NIPAM thermo-sensitive functionalities has many disadvantages. One of these disadvantages is the necessity of the incorporation of a high-cost coupling agent in the polymer synthesis and the need for some inorganic salts to initiate the thermal-aggregation which increases the cost of this type of polymer (Li et al., 2017a; Su and Feng, 2018). The usage of petroleum-based chemicals for the synthesis of these thermo-sensitive monomers increases the environmental concerns of these polymers and increases their manufacturing cost. The low molecular weight of the synthesized TVP polymers makes these polymers cannot afford a significant increase in the viscosity at the required concentration and a higher polymer concentration is required to attain the desired increase in viscosity (Tamsilian et al., 2020; Li et al., 2017a).

Limited research trials were recently reported to overcome these limitations. Chen et al. (2013) stated the preparation of TVP polymer by copolymerization of MPAD thermo-responsive monomer, which was prepared from N-(1,1-dimethyl-3- oxobutyl)-acrylamide (DAAM), with acrylamide (AM). The prepared TVP has a moderate molecular weight of 8.2×10^6 g/mol and increased the oil recovery factor to 13.5 % at a salt concentration of 32,868 ppm at 85 ºC. Li et al. (2017a) concluded that (AM-co-MPAD) TVP copolymer can increment oil recovery by 15.5 % at a salinity of 101,000 ppm and 85 ˚C. Akbari et al. (2017a) reported the preparation of AM and 2-acrylamido-2-methyl propanesulfonic acid (AMPS) copolymer with a molecular weight of 12×10^6 g/mol. The prepared TVP copolymer showed a thermo-responsive behaviour at brine salinity of (1,000 ppm–100,000 ppm). The rheological properties of the prepared copolymer were then evaluated at 80 ºC for varying aging times ranges from zero to 90 days in the presence and absence of isobutyl alcohol (IBA) as an antioxidant (Akbari et al., 2017b). These studies were performed at temperatures up to 85 ˚C and an average salinity of l01,000 ppm where TVP concentration of at least 0.2 wt.% was required to observe thermo-responsive behavior and increase oil recovery, no studies were reported so far approaching a synthesis of TVP polymer with higher molecular weight

using a green cost-effective route for EOR application at extremely harsh reservoir conditions of total dissolved solids (TDS) 230,000 ppm and 100 °C. According to the literature no studies were reported about the application of ultra-low TVP polymer concentrations for EOR application at hostile reservoir conditions.

In this context, the present research reported on the utilization of WVO to synthesize a novel high molecular weight TVP that overcomes the limitation of the existing TVPs for EOR application. A novel environmentally benign, cost-effective thermo-sensitive oleic phenoxypropyl acrylate (OPA) monomer synthesized from WVO *via* a green route transesterification reaction then copolymerized with poly (acrylamide/ 2-(acryloyloxy)ethyl]trimethylammonium chloride /Acrylamido-2-methyl-1-propanesulfonic acid) terpolymer in presence of dimethylphenylvinylsilane through direct free radical polymerization. The incorporation of the newly synthesized monomer acted as thermo-sensitive blocks resulting in a high molecular weight polymer composite with pronouncing thermo-responsive behaviour even in salt-free solutions and ultra-low polymer concentrations. The synthesized polymer composite was assessed for EOR applications by conducting displacement experiments using sandstone cores at simulated hostile reservoir conditions of 100 ºC and a salinity of about 230,000 ppm the recovery factor was determined. The capability of the synthesized nanocomposite to alter the wettability of sandstone rock surface from oil-wet to water-wet was assessed by measurement of contact angle. This novel thermo-sensitive monomer and polymer nanocomposite have not been previously introduced in the literature. Therefore, this research presents a concept for the adaptation of WVO into valuable green high molecular weight thermo-sensitive nanocomposite for EOR application at hostile reservoir conditions.

2. Experimental

The used material and synthesis procedure of the thermo-responsive monomer and green thermo-sensitive nanocomposite have been introduced in this section. The characterization techniques and core flooding experiments details have been discussed.

2.1 Materials

WVO collected from restaurants in Egypt; 2-hydroxy-3-phenoxypropyl acrylate; N,N- dimethyl sulfoxide (DMSO ≥ 99.9 %); 4-(dimethylamino)pyridine (DMAP≥98.0 %); acrylamide (AM ≥99 %); 2-Acrylamido-2-methyl-1-propanesulfonic acid (AMPS ≥99 %); sodium dodecyl sulphate, (SDS ≥ 98.5 %); 2-(acryloyloxy)ethyl]trimethylammonium chloride (DAC, 80 wt.% in water); dimethylphenylvinylsilane (98 %); potassium persulfate (KPS ≥ 99 %); ethanol ultra-pure; acetone (≥97 %); chloroform (≥97 %); sodium azide (NaN_3, ≥99.5 %); dimethyl sulfoxide-d_6 (99.9 atom %D). All chemicals were supplied by Sigma-Aldrich.

2.2 Synthesis of oleic phenoxypropyl acrylate monomer (OPA)

The transesterification reaction was carried out to convert triglycerides of WVO to fatty acid methyl esters (FAME). The experimental procedure is discussed in detail elsewhere (Aboelazayem et al., 2018). The synthesis of oleic phenoxypropyl acrylate thermo-sensitive monomer was carried out by the transesterification reaction between the functional hydroxyl group of 2-hydroxy-3-phenoxypropyl acrylate and FAME. In 250 ml double-walled reactor equipped with a mechanical stirrer, thermometer, and condenser. 12 g of 2-hydroxy-3- phenoxypropyl acrylate, 15 g of WVO, and 15 ml of dimethyl sulfoxide were added and mixed. The temperature of the reaction mixture

was then increased to 45 °C in the presence of 4-(dimethylamino)pyridine as a catalyst with stirring. The reaction mixture was stirred at 45 °C for 6 hours. The synthesized product was then mixed with dichloromethanethane then washed 5 times with brine and ethanol. A flow chart summarizes the experimental procedure for the synthesis of AGPC nanocomposite is indicated in Figure S1 (supporting information). The transesterification reaction mechanism of FAME and 2-hydroxy-3- phenoxypropyl acrylate is shown in Figure 1.

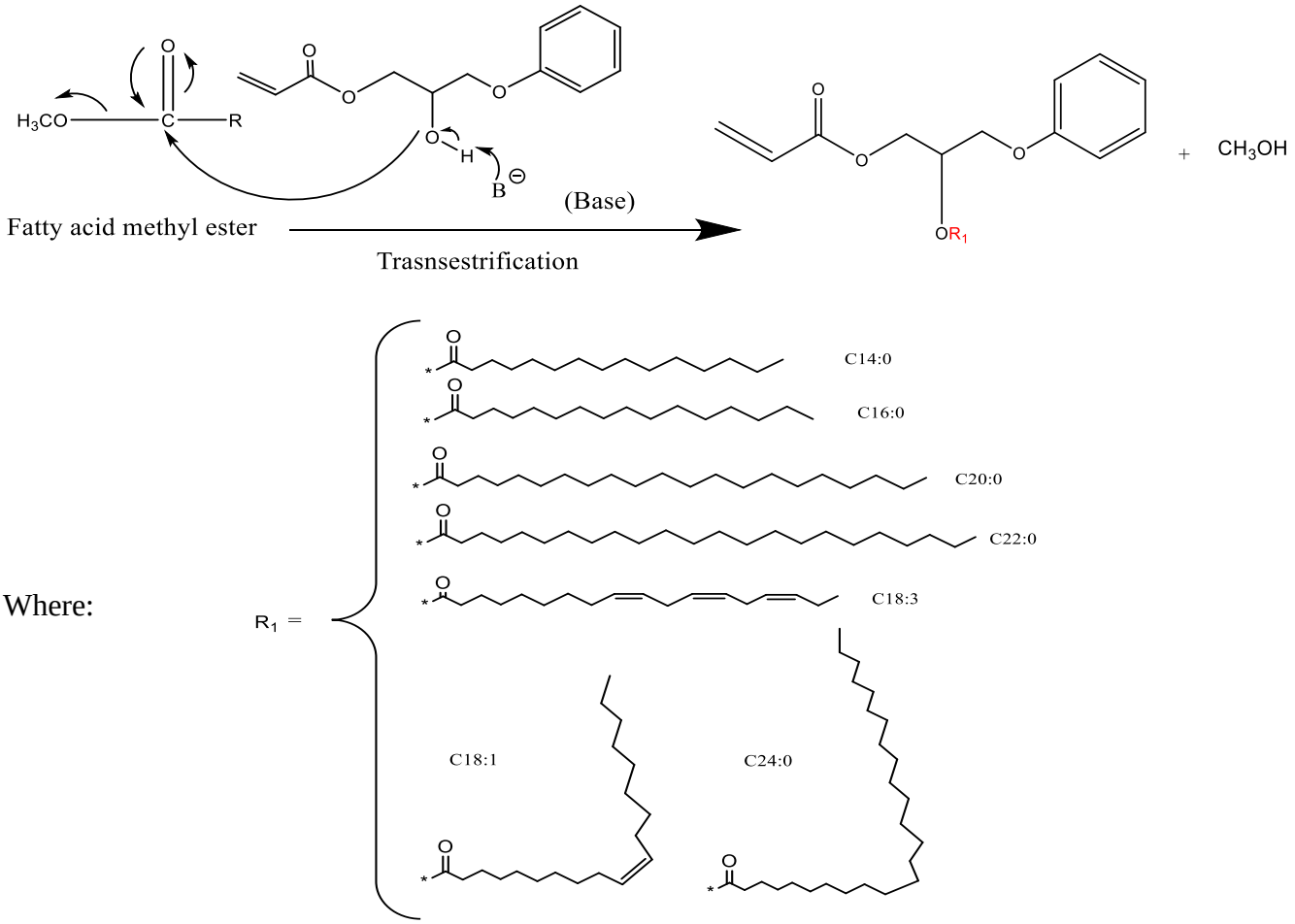

Figure 1. Transesterification of FAME with 2-hydroxy-3- phenoxypropyl acrylate reaction mechanism

2.3 Synthesis of amphoteric green polymer functionalized silica composite (AGPC)

After the preparation of the OPA thermo-sensitive monomer, the typical emulsion polymerization procedure was performed in a four-neck 250 ml reactor with a mechanical stirrer, nitrogen inlet/outlet, thermometer, and condenser. The anionic surfactant SDS was dissolved in deionized water and charged into the reactor. The designed amount of prepared (OPA), acrylamide, 2-(acryloyloxy)ethyl]trimethylammonium chloride, and 2-acrylamido-2-methyl-1-propanesulfonic acid monomers were added into the reaction mixture and stirred vigorously and purged with nitrogen for 30 min. The mixture was heated to the designated reaction temperature; then potassium persulfate and dimethylphenylvinylsilane were added to the reaction mixture. The copolymerization reaction proceeded under N_2 for 12 hours. The obtained polymer gel was

precipitated by acetone and subsequently washed with ethanol and Soxhlet extraction using chloroform for 24 hours. The obtained polymer was then dried at 60 °C for 24 hours. During the emulsion polymerization process, micelles between fatty acid hydrophobic groups of the polymer and SDS molecules were formed. The concentration of reactants along with polymerization conditions are summarized in Table 1.

Table 1. Concentration of reactants and polymerization conditions.

A	B	C	D	E	F	G	H
1.89	$1.57*10^{-1}$	$10.8*10^{-2}$	$1.158*10^{-1}$	$4.43*10^{-3}$	$8.87*10^{-3}$	12	60

A; Acrylamide monomer concentration, mole L^{-1}. B; OPA monomer concentration, mole L^{-1}. C; DAC monomer concentration, mole L^{-1} D; AMPS monomer concentration, mole L^{-1}. E; KPS initiator concentration, mole L^{-1}; F; dimethylphenylvinylsilane, mole L^{-1}. G; Reaction Time, Hours. H; Reaction Temperature, °C.

2.4 Solutions of brine and displacing fluids

Brine solutions with different salinities were prepared from double distilled water. Table 2 summarizes the composition of saline solutions used in the measurements of rheological properties.

Table 2. Composition of saline solutions used in rheological properties measurements.

Ions	Ions concentration, g/L							
Total dissolved solids (TDS)	5	10	20	40	80	100	150	230
Na^{+}-ion(NaCl), gL^{-1}	4.66	9.32	18.65	37.31	74.62	93.28	139.92	214.54
K^{+}-ion (KCl), gL^{-1}	0.037	0.074	0.14	0.29	0.59	0.74	1.11	1.70
Mg^{+2}-ion ($MgCl_2.6H_2O$), gL^{-1}	0.075	0.15	0.30	0.60	1.20	1.5	2.25	3.45
Ca^{+2}-ion ($CaCl_2.2H_2O$), gL^{-1}	0.22	0.44	0.89	1.79	3.58	4.48	6.72	10.30

2.5 Characterization techniques

The physical and chemical properties of WVO feedstock synthesized OPA monomer and AGPC nanocomposite were identified using various characterization methods. Standard methods were applied to characterize the physicochemical properties of WVO, which include ASTM D-4052 to measure density and ASTM D-974 method- to measure - total acid number (TAN)-. The investigated properties were measured two times and the results were calculated by averaging the two obtained results. The composition of fatty acids contained in WVO feedstock was analysed by converting them to methyl esters using BS EN ISO 12966-2:201. The derivatised WVO sample

was analysed for the content of methyl ester using GC-MS (Shimadzu GCMS-QP2010S) with a capillary column (TR-BD 30 m × 0.25264 mm × 0.25 μm). The temperature started from 50 °C for 1 min. then it was ramped at 20 °C /min to 200 °C for 5 min then increased with 3 °C/min to 230 °C for 23 min. The temperatures of the injector and detector were held at 250°C. Mass spectra with a range of m/z 20-550 were used to identify the methyl esters content by using the spectrum fragmentation patterns that are available in NIST Mass Spectral Library data.

The infrared spectra analysis was carried out using a Shimadzu FTIR-8400 infrared spectrometer with a KBr beam splitter at a scanning range of 400-4000 cm^{-1}. 32 scans with a spectral resolution of 6 cm^{-1} were performed for better clarity of the recorded infrared spectra. The ^{1}HNMR analysis was carried out on Bruker Avance 400 spectrometer (Bruker, Rheinstetten, Germany) run at 400 MHz using deuterated DMSO as solvent. The particle size distribution of AGPC particles was measured by Marven Zetasizer equipped with a He–Ne laser and cuvette rotation/translation unit (CRTU). Thermogravimetric analysis was achieved using a thermogravimetric analyzer (Shimadzu TGA-50). The temperature reproducibility of the TGA instrument is ±2.1 ºC. The analysis was done in a nitrogen atmosphere in the temperature range of 25 ºC to 600 ºC using a heating ramp of 10 ºC min^{-1}. The morphological analysis of polymer samples was achieved using Field Emission Scanning Electron Microscope (Hitachi S-4800 II Model). Polymer samples were coated by Sputter Coater E-1010. Bruker Energy Dispersive X-ray spectrometer (QUANTAX 200 model) was used to perform elemental analysis for the synthesized polymer composite. TEM images were captured on JEM-2100F high-resolution transmission electron microscope operating at 200 kV. The molecular weight was determined by gel permeation chromatography (GPC) comprising of a Waters 515 HPLC pump and a Waters 2410 Refractive Index (RI) detector. The rheological properties of the prepared composite were estimated using a Marven Gemini rheometer equipped with a cone and a 40 mm diameter plate equipped with a solvent trap. The apparent viscosity of nanocomposite solutions was studied as a function of concentration, salinity, temperature, and shear rate. The salt resistance experiments were evaluated using synthetic seawater with different salt concentrations ranging from 5,000-230,000 ppm. The contact angle was measured by a goniometer equipped with a Leica Wild M3Z microscope and a JVC TKC1381 camera. The configuration of the oil drop was studied by First Ten Angstroms Incorporated Drop Shape Analysis Software.

2.6 Permeability reduction and polymer adsorption

The ability of polymer solutions to flow smoothly in reservoir pore spaces is evaluated through the determination of the resistance (R_f) values using Equation (1) and residual resistance factors (R_{rf}) using Equation (2) by reporting the pressure differential throughout the core flood experiments (Liu et al., 2018). The core is saturated with synthetic brine (230,000 ppm), then polymer solution is injected until pressure is stabilized followed by brine injection until pressure is stabilized again. All runs are conducted at 100 ºC, and pressure difference is reported. Resistance factor (R_f) is the effective viscosity of the polymer compared to brine in pore spaces and is used to express the polymer's capability to decrease the mobility ratio (Zhong et al., 2016). Whereas residual resistance factor (R_{rf}) is utilized to characterize the adsorption of the polymer molecules in porous media and displays the ability of the polymer to reduce water permeability (Liu et al., 2018). It is also worth mentioning that higher values of R_f and R_{rf} promote a greater enhancement of displacement efficiency which is favorable to improving the efficiency of the polymer flooding process. Yet excessive values of these factors are not required as core-plugging and injectivity problems during polymer flooding may happen (Donaldson et al., 1989).

$$R_f = \left(\frac{K_W / \mu_w}{K_p / \mu_p} \right) = \frac{\Delta P_p}{\Delta P_w} \quad (1)$$

$$R_{rf} = \left(\frac{K_W}{K_{wp}} \right) = \frac{\Delta P_{wp}}{\Delta P_w} \quad (2)$$

The thickness of the adsorbed polymer layer, ξ, was calculated using equations (3) and (4) (Zaitoun and Kohler, 1988; Song et al., 2015) where: r_p is the average pore radius; φ is the porosity of the core, fraction; and k_e is the brine permeability, Darcy, ζ / r_p is the extent of polymer retention in porous medium, %.

$$r_p = \left(\frac{8 K_e}{\phi} \right)^{1/2} \quad (3)$$

$$\xi = r\left(1 - R_{rf}^{-1/4}\right) \quad (4)$$

2.7 Flooding experiment

Core flooding experiments were conducted on a flooding setup designed to simulate the displacement process under reservoir conditions as shown in Figure 2. The core flooding setup equipped with three accumulators were charged with AGPC nanocomposite, brine, and crude oil; a Presearch Limited model 260D syringe pump and Bronkhorst EL-PRESS pressure meter. The experimental procedure was initiated by core preparation at which a standard Berea sandstone dried core was weighted, and core dimensions were reported. The core is saturated with synthetic brine (230,000 ppm) under vacuum and the pore volume was calculated by estimating and dividing the volume of brine imbibed inside the core by the brine density. The core porosity was then calculated by dividing the estimated pore volume by the total core volume (Alshibli et al., 2006; Alramahi et al., 2005). The saturated core was then located inside the core holder (500 psi, 100 ^{o}C) where it is connected to the accumulators. Brine was then injected with varied flow rates (10, 8, 6 and 3 mL/min) while the pressure differential is reported, and absolute permeability was calculated at each flow rate using Darcy's law. Crude oil is then injected into the core until the water cut was less than 2.0 %. The volume of produced water is divided by the pore volume to estimate the initial oil saturation. Brine injection was continued until a water cut of 98 % is reached, then polymer flooding was initiated. The cumulative oil recovery and the volume of recover water-related injected pore volume and post-water flooding were utilized to assess the efficiency of the polymer displacement process. The pressure differential along the core throughout the flooding process was reported. The physical properties of sandstone cores are summarized in Table 3.

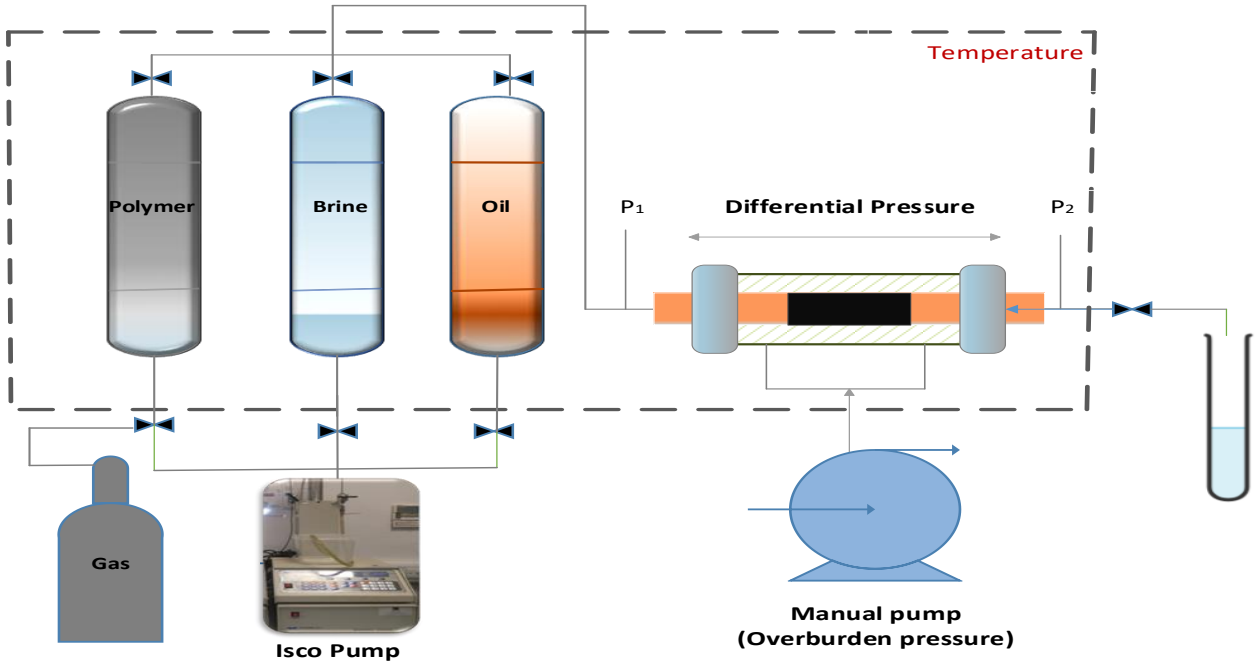

Figure 2. Schematic illustration of core flooding system.

Table 3. Physical parameters of sandstone core during the core flooding experiments.

Core sample	Diameter, cm	Length, cm	Bulk volume, cm^3	Dry weight, g	Pore volume, cm^3	Porosity, %	Brine permeability, mD	Initial oil saturation (S_{oi}), %	Residual water saturation (S_{wr}), %
Core#1	3.814	6.72	76.77	171.94	11.4±0.08	14.84±0.5	521±3.0	73.6±0.1	26.4±0.1
Core#2	3.814	6.72	76.77	175.90	11.1±0.08	14.45±0.5	510±3.0	73.8±0.1	26.1±0.1
Core#3	3.814	6.92	79.06	176.80	11.9±0.1	15.05±0.4	537±3.0	72.2±0.1	27.7±0.1

3. Results and discussions

The results of the characterized WVO synthesized APO thermo-sensitive monomer and AGPC nanocomposite have been discussed in this section. Further investigations on the AGPC solutions that involve rheological properties at varied conditions, core flooding experiments ,and recovery estimation along with wettability assessment have been discussed in detail.

3.1 Physicochemical properties of WVO feedstock

Standard methods were applied to characterize the physicochemical properties of WVO, which include ASTM D-4052 to measure density and ASTM D-974 to measure total acid number (TAN). Table 4 summarizes the measured density and TAN values of WVO feedstock.

Table 4: physicochemical properties of WVO feedstocks.

Petrophysical properties	Method	[a]Oil Feedstock
Density g/cm^3	ASTM D-4052	0.93
[b]TAN mg KOH g^{-1}	ASTM D-974	10

[a] Properties were measured two times, and the results were calculated by averaging the two reported results. [b]TAN is the amount of potassium hydroxide (mg) required to neutralize the acidity of one gram of oil.

3.2 Gas chromatography-mass spectrometry (GC-MS) analysis

To define the main components of the WVO that was used in OPA monomer synthesis, WVO was firstly derivatised and then injected into the GC-MS analyser. Figure 3 shows the GC-MS chromatogram of the derivatised WVO, where the solvent peak of *n*-hexane was excluded for better clarity. Seven major components were defined including methyl tetradecanoate (C14:0), methyl-palmitate (C16:0), methyl-oleate (C18:1), methyl -linolenic (C18:3), methyl eicosanoate (C20:0), methyl docosanoate (C22:0) and methyl tetracosanoate (C24:0). These results are in good agreement with other published literature (Chuang et al., 2013).

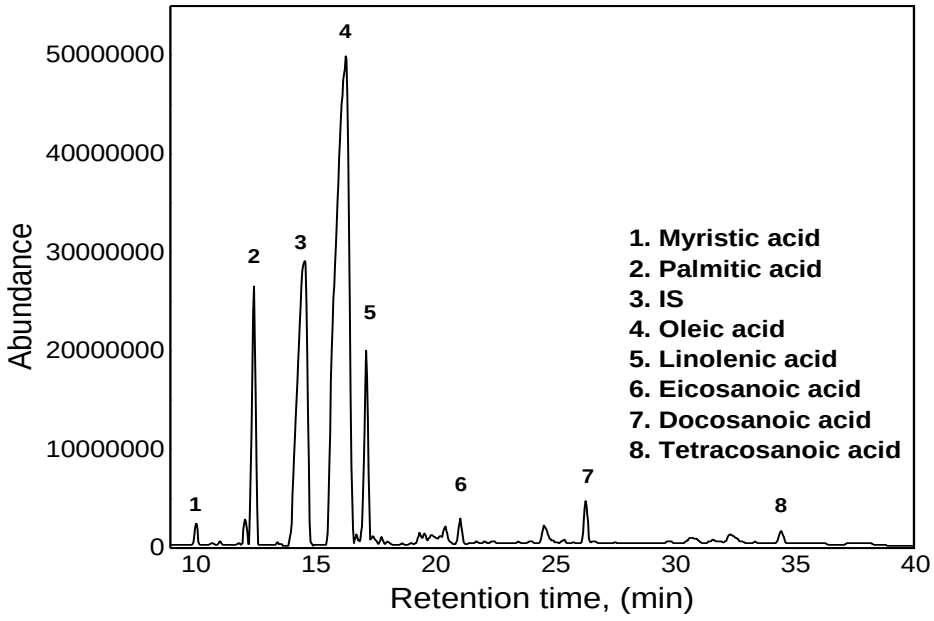

Figure 3. GC-MS chromatogram of derivatised WVO.

3.3 Spectroscopic analysis and molecular weight determination

FT-IR spectra of WVO feedstock and the synthesized thermo-sensitive monomer OPA are presented in Figure 4. It can be observed that the FT-IR spectrum of WVO shows characteristic absorption peaks at 3010.20 cm^{-1} which is assigned to the *cis* olefinic C-H double bond. The characteristic peaks at 2851.91 m^{-1}, and 2920.30 cm^{-1} are attributed to (C-H) stretching vibration the of saturated carbon-carbon bond. The band at 1745.10 cm^{-1} is due to the presence of carbonyl's stretching vibration of triglycerides (C=O). A small peak at 1656.69 cm^{-1} is due to the *cis* (C=C) double bond. The absorption peaks at 1463.79 cm^{-1} were assigned to CH_2 and CH_3 aliphatic groups. The weak absorption band at 966 cm^{-1} is due to the presence (C-H) of unsaturated free fatty acids (Al-Degs et al., 2011; Yang and Irudayaraj, 2000). The FT-IR spectroscopy of the synthesized thermo-sensitive monomer OPA shows the presence of a strong C=C adsorption peak at 1560 cm^{-1}, the carbonyl peak at 1630 cm^{-1} and the ester C=O peak at 1750 cm^{-1}, which indicate the attachment of vinyl and ester groups to the fatty fragment. The observed strong ester peak at 1750 cm^{-1} proves the ester nature of the synthesized thermo-responsive monomer.

The infrared spectrum of the polymer nanocomposite AGPC is indicated in Figure 5. The characteristic vibration absorption peaks of $–NH_2$ appeared at 3416.3 cm^{-1} and carbonyl's stretching at 1665.9 cm^{-1} in amide group $O=CNH_2$ which proves the existence of acrylamide segments in the synthesized polymer composite. The –COO absorption peak from esters groups appeared at 1740 cm^{-1}, which proves the incorporation of the OPA monomer. The absorption peaks of methylene $-CH_2-$ appeared at 2800 cm^{-1} and methyl groups $-CH_3-$ at 2930 cm^{-1} that signifies the presence of the fatty acid chains (Quan et al., 2016; Wu et al., 2017). The characteristic peaks at 1449 cm^{-1}assinged to methyl groups linked with ammonium, and the absorption peak at 952 cm^{-1} attributed to $N^+(CH_3)_3$ stretching vibration in 2-(acryloyloxy)ethyl]trimethylammonium chloride. The presence of these two peaks proves the incorporation of cationic moieties into the copolymer backbone. The $–SO_3–$ absorption peaks at 1192.2 cm^{-1} and 1042.5 cm^{-1}, prove that the synthesized polymer has AMPS segments. The absorption peaks at 1265-1120 cm^{-1} and 600 cm^{-1} are assigned to (Si-O-Si) in the silica nanoparticles (Hayakawa and Hench, 2000). The absence of a characteristic band of the vinyl group from 1600–1650 cm^{-1} confirms successful and complete polymerization.

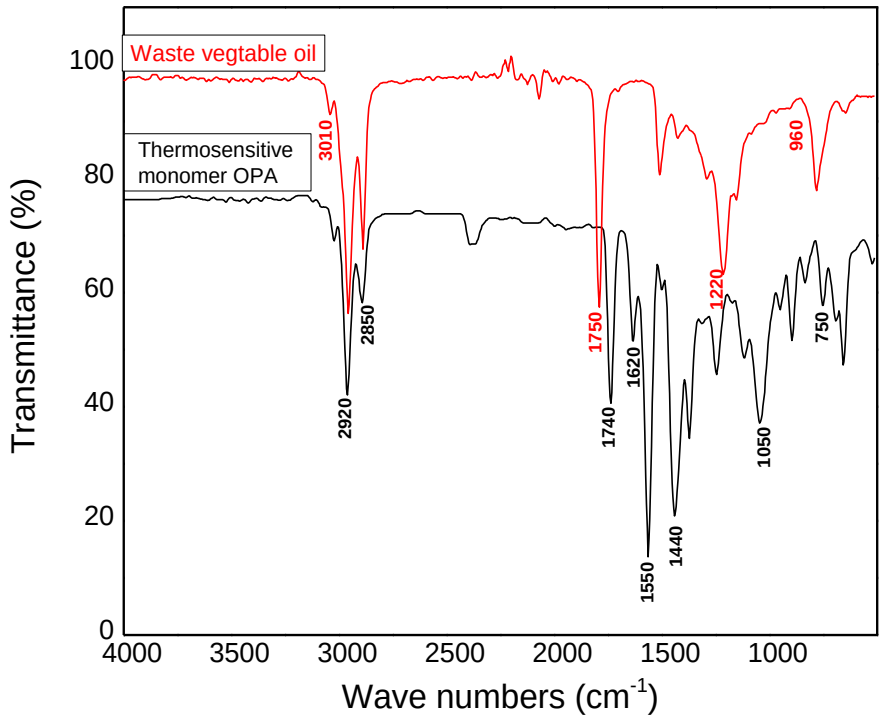

Figure 4. Fourier Transformation spectroscopy (FTIR) of WVO feedstock and OPA thermosensitive monomer.

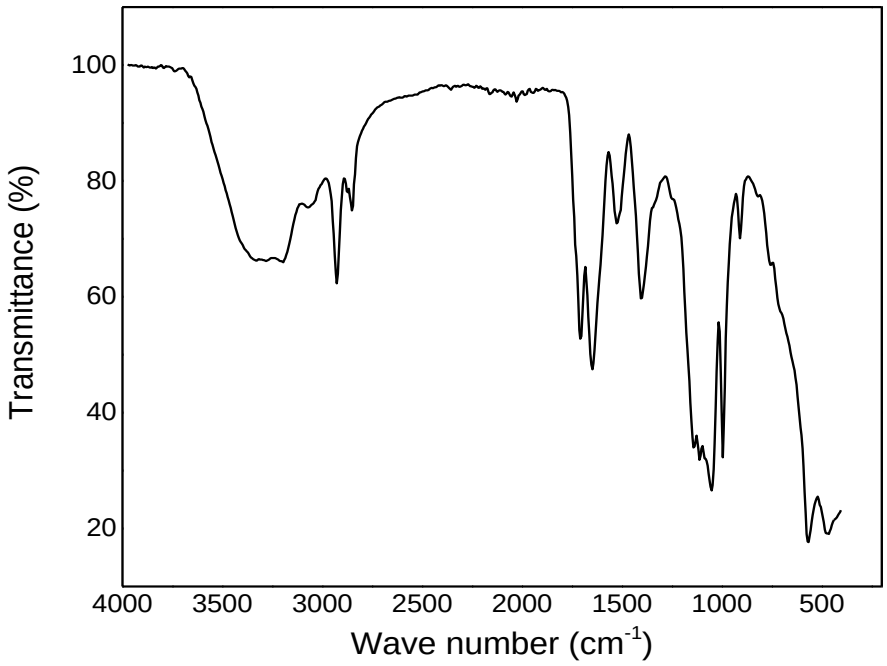

Figure 5. Fourier Transformation spectroscopy (FTIR) of synthesized AGPC nanocomposite.

The structure of the synthesized compounds was confirmed using ^{1}H NMR spectroscopy. ^{1}H-NMR (400 MHz, DMSO) of the synthesized compounds is shown in Figure 6. The ^{1}H-NMR spectrum of the thermo-sensitive monomer OPA exhibit a chemical shift at 0.87, which is assigned to the three protons of the terminal methyl group of the fatty acid chain. The characteristic chemical shifts at 2.3 correspond to the methylene group near the newly formed carbonyl group due to the transesterification reaction (2H, C(O)-CH_2-CH_2). The peak at 1.6 ppm can be assigned to the protons of the methylene group directly after it. The signals at 1.26 represent methylene groups protons (18H, -CH_2-) in the aliphatic side chains. The signals at 5.3 ppm correspond to the isolated double bond protons (-CH=CH-). The peaks between δ (ppm) =5.8-6.8 are attributed to the three protons of acrylic double bond (-CH=CH_2). The characteristic peak at 5 ppm represents the geminal proton close to the newly formed carbonyl groups (CH_2=CH-C(O)). The obvious peaks at 2.3 ppm and 5 ppm prove successful transesterification reactions. A ^{1}H-NMR spectrum of polymer nanocomposite AGPC displays chemical shift at δ (ppm) = 0.26, which corresponds to the protons of the two-terminal methyl group attached to the silica atom in dimethylphenylvinylsilane. The asymmetric peaks at δ = 1.39 ppm was attributed to the protons at the backbone of methylene and the peak at δ = 2 ppm was attributed to methane groups another peak at 1.4 ppm represents the six protons of a methyl group (6H, -CCH_3**)** of AMPS. The chemical shift δ = 3.1 ppm represents the methyl group protons of -N^+-$(CH_3)_3$, and the two peaks at δ = 3.40 ppm and δ = 4.5 ppm represent the methylene groups protons of -CH_2-N^+- and -O-CH_2- of DAC. The chemical shifts at δ (ppm) =7.08–7.29 assigned to (–CH=CH-) at the phenyl ring in dimethylphenylvinylsilane. The absence of chemical shift between 5.8-6.8 ppm, which corresponds to the acrylic double bond (-CH=CH_2) and confirms complete monomers polymerization. Table 5 summarizes the characteristic peaks and assignment details of the synthesized OPA thermo-sensitive monomer and polymer nanocomposite AGPC by FTIR and ^{1}H NMR methods.

a

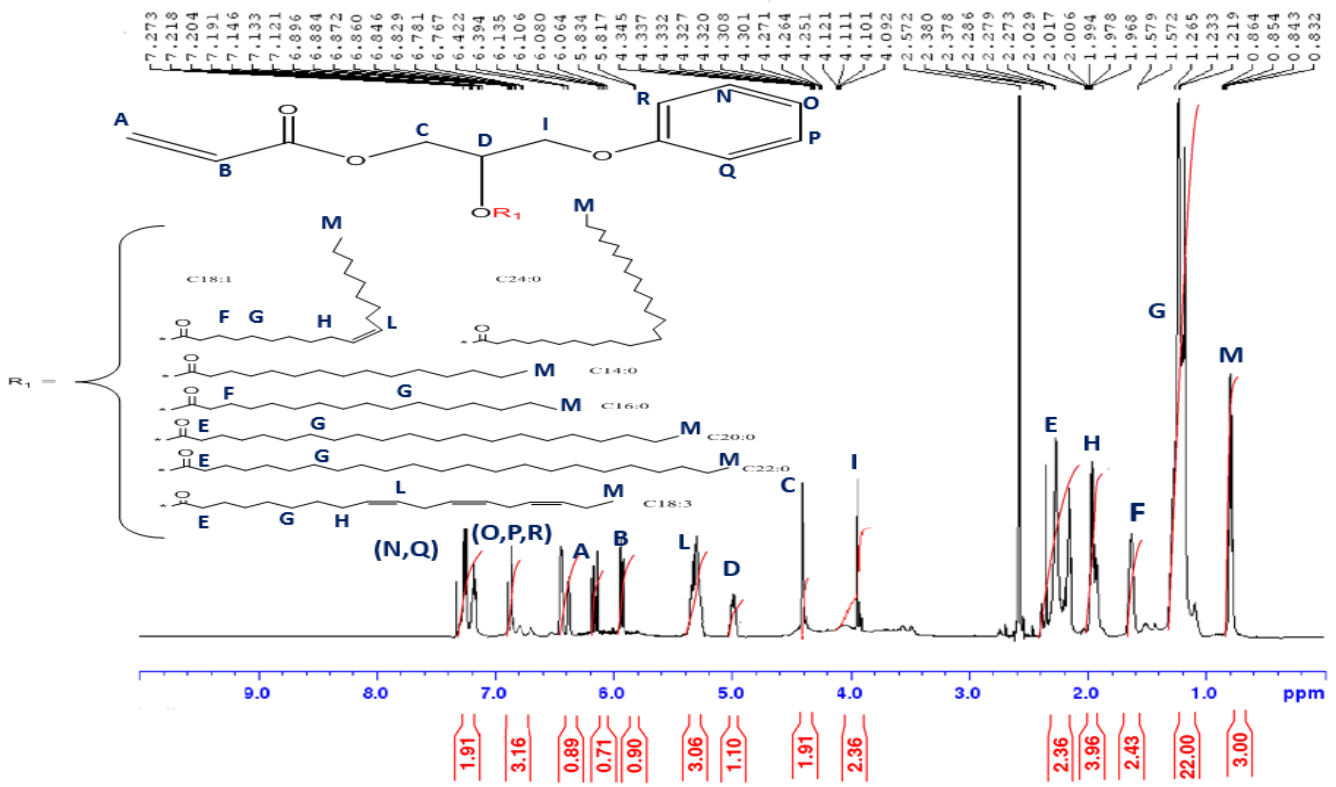

b.

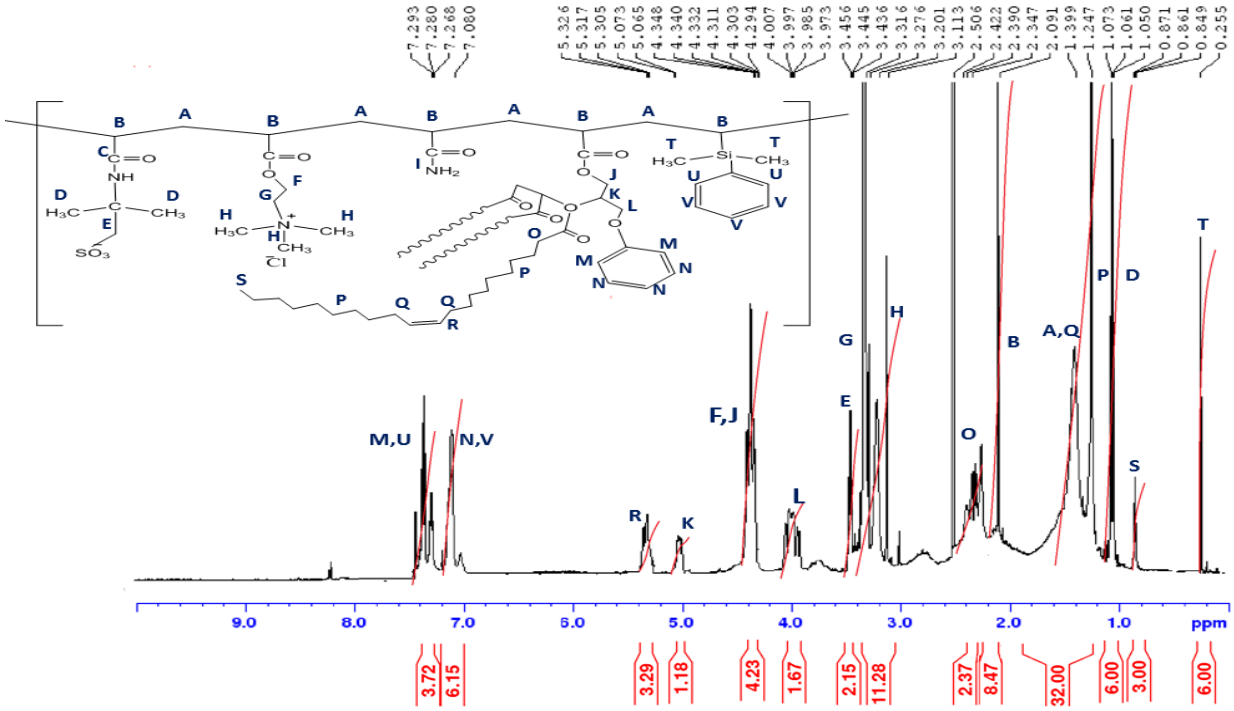

Figure 6. (a) Proton ^{1}H NMR spectra of OPA thermo-sensitive monomer and (b) polymer nanocomposite AGPC.

505 Table 5. Summary of spectroscopic characterization data of OPA thermo-sensitive monomer and
506 polymer nanocomposite AGPC.

	Thermosensitive monomer OPA		Polymer nanocomposite AGPC	
Analysis	Frequency, cm^{-1}	Assignments	Frequency, cm^{-1}	Assignments
FTIR bands	3010	=CH, CH_2, alkene)	3400-3200	Stretching vibrations of - NH_2 in the amide groups.
	2927	C-H, stretches	2870-2930	(CH_2, alkane)
	2850	CH_2-, alkane	1740	C=O, ester)
	1750	C=O, ester	1657	(C=O, amide I)
	1630	C=C, vinyl	(1449.7&950.7)	–CH–$N^+(CH_3)_3$
	1560	C=C, aromatic symmetric C=O stretching (carboxyl group)	1240	(C-C(O)-O, ester)
	1440	C-H deformations, CH_2 or CH_3 groups	(1192.2&1042.5)	$–SO_3H^-$, antisymmetric stretching (sulfonyl group of AMPS)
	1245	C-C(O)-O, ester	(1120&600)	(Si-O-Si)
	750	C-H, benzene		
^{1}H-NMR	Chemical shift (δ) ppm		Chemical shift (δ) ppm	
	0.87 (3H, CH_2-CH_3) terminal –CH_3 group 1.26 (15-22H, (CH_2)) 1.6 (2H, C(O)-CH_2-CH_2) 2.10 (4H, CH_2-CH=) 2.3 (2H, C(O)-CH_2-)		0.26 (s, 6H, –CH_3-Si- CH_3-) terminal two CH_3 groups	
			0.87 (3H, CH_2-CH_3) terminal –CH_3 group 1.23-1.6 (22H, -CH_2-) methylene groups	
	4-4.5 (2H, CH_2-O-) 5 (1H, CH_2=CH-C(O)) 5.21 (2-3H, CH=CH)		3.5(2H, $-CH_2SO_3^-$), 1.073(6H, -CCH_3) of AMPS 3.1 (9H, -N^+-$(CH_3)_3$, 3.34(2H, -CH_2N^+-)	
	5.8-6.8(1H, HCH=CH-C(O))		4.5 (2H, -O-CH_2-) of DAC 7.08–7.3 (5H, –CH=CH-) of dimethylphenylvinylsilane	
	7.08–7.3 (d,5H, –CH=CH-) at the phenyl ring			

507
508

The average molecular weight and dispersity index Đ for OPA thermoresponsive monomer was measured with gel permeation chromatography (GPC) with a Waters 515 HPLC pump and a Waters 2410 Refractive Index (RI) detector and a set of four Styragel HR columns, the temperature of the column were adjusted to 40 °C. The HPLC grade tetrahydrofuran (THF) was used as a carrier eluent. The measured molecular weight of OPA thermoresponsive monomer is 425 g/mol and the dispersity index is 1.25. The molecular weight of the AGPC nanocomposite was determined using an ultrahydrogel linear column. Dried AGPC nanocomposite was dissolved in deionized water stabilized with sodium azide then the obtained solution was filtered by a Teflon membrane filter with a pore size of 0.45 mm. The analysis was performed at 25 ºC and a flow rate of 1 ml/min. The measured molecular weight of AGPC nanocomposite was 2.3x10^7 g/mol. A dynamic light scattering approach was applied to estimate the molecular weight of the AGPC nanocomposite by constructing a Debye plot as indicated in Figure 7. Table 6 summarizes K_C/R_{op} values for different concentrations of AGPC nanocomposite along with the calculated molecular weight using the Debye plot and the measured molecular weight values the using GPC technique.

Table 6: K_C/R_{op} values for different concentrations of AGPC nanocomposite along with calculated and measured molecular weight of AGPC nanocomposite.

Concentration g/ml	K_C	K_C/R_{oP} 1/kDa	Molecular weight, g/mol	
			Calculated	Measured
$1.00E^{-5}$	3920	$8.00E^{-5}$	2.5x10^7	2.3x10^7
$5.00E^{-5}$	3029.4	$6.20E^{-5}$		
$3.00E^{-4}$	5544.4	$3.00E^{-4}$		
$4.00E^{-4}$	3651.8	$4.43E^{-4}$		

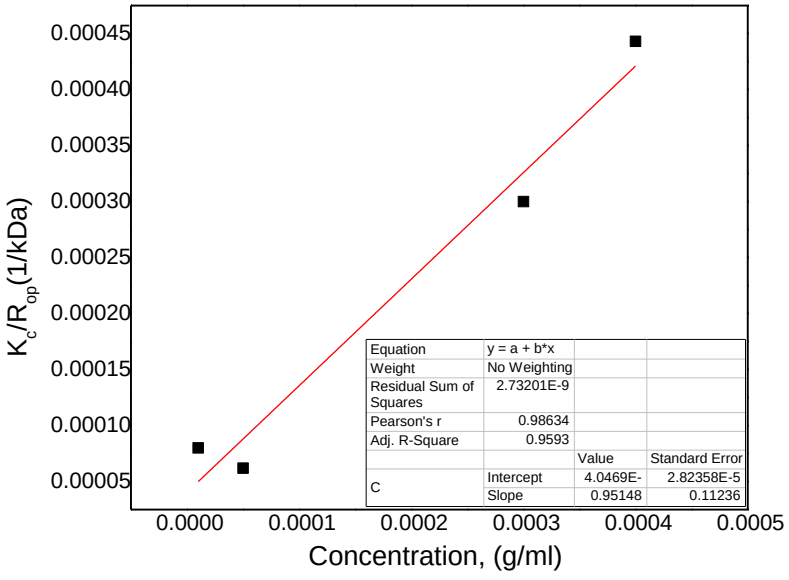

Figure 7. Debye plot for molecular weight calculation of AGPC nanocomposite *via* dynamic light scattering technique.

3.4 Thermal gravimetric analysis (TGA) and differential thermal analysis (DTA)

The TGA and DTA curves of four nanocomposite samples prepared with different OPA monomer content are shown in Figure 8. As indicated in TGA curves for both amphoteric polymer composite (APC) with zero OPA monomer content and AGPC nanocomposite samples prepared with different concentrations of OPA monomer (AGPC/OPA) there are three regions for thermal decomposition. The onset degradation temperature of the APC sample at which a mass loss of 10 % was reached (T_{10} %) was ~100 ºC, while the second thermal degradation was at 120-385 ºC showing a weight loss of ~66 %, and the last weight loss of ~10 % was observed from 358 ºC to 450 ºC. The corresponding area of the first decomposition stage occurs due to the loss of intra and intermolecular water on the DTA curve is proved by a small peak on the left. The second decomposition stage is due to the thermal decomposition of the APC from high molecular weight macromolecules to smaller chain fragments. The third weight loss stage happens due to the complete thermal decomposition of APC. Additionally, it can be observed that the incorporation of OPA monomer significantly increased the thermal stability of the prepared composite, which is evidenced by the considerable increase in T_{10} and T_{50} values and markedly decrease of the second and third peaks on the DTA curve by increasing the OPA monomer feed composition. The reported temperatures of the maximum DTA peaks (T_{max}) for AGPC polymer increase with increasing OPA monomer incorporation as shown in Figure 8 (b). For instance, the TGA curve of AGPC/OPA0.016 showed that the main thermal degradation stage started at 300 ºC and ended approximately at 460 ºC with a weight loss of 30 % which is 36 % lower than the APC sample. The thermal decomposition in this stage can be attributed to the decomposition of the hydrophobic fatty acid chains besides the degradation of the polymer chains which normally involves the breakage of C–H, C–C, N-O, and C–O bonds. The reported (T_{10}) increased to 210 ºC and (T_{max}) to 495 ºC, which convey improved thermal stability by the addition of OPA monomer. Compared with AGPC/OPA0.016 composite, lower thermal stability was noted for the composite samples with lower content of OPA monomer such as AGPC/OPA0.0047 in which the (T_{max}) value reduced to around 442 ºC and AGPC/OPA0.0094 in which the (T_{max}) value is 473 ºC. This thermal stability improvement of the green composite containing OPA monomer is related to the fatty acid fragments formed by OPA monomer.

a.

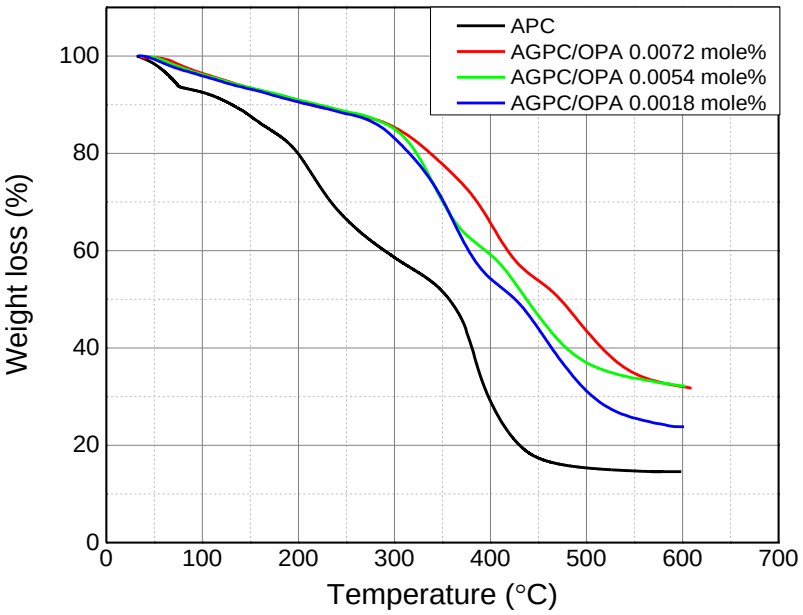

b.

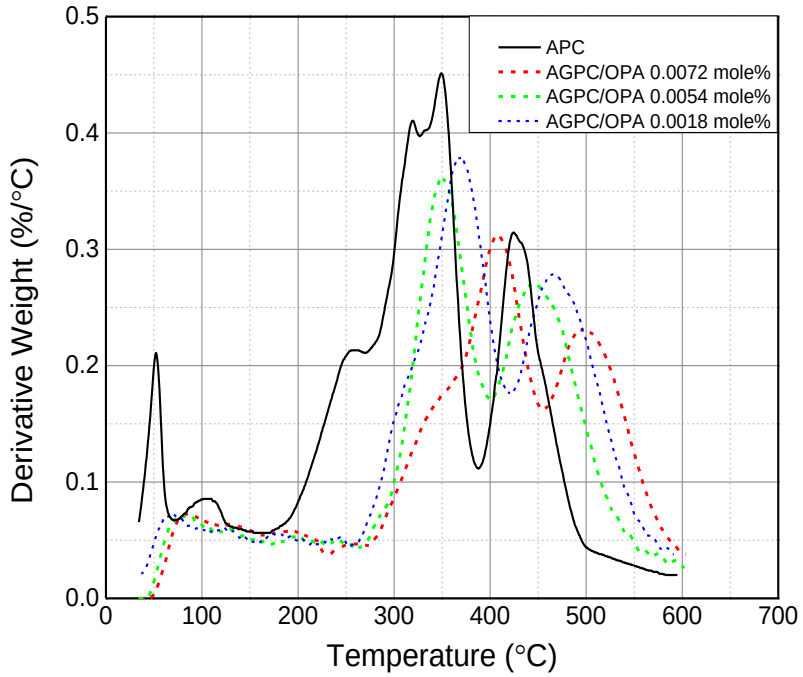

Figure 8. (a) Thermogravimetric analysis (TGA) and (b) differential thermal analysis (DTA) of polymer samples synthesized using different content of thermo-sensitive monomer OPA.

3.5 Scanning electron microscopy (SEM) and energy dispersive X-Ray (EDX) spectrometry analysis

The surface morphology of different polymers with various monomer compositions is shown in Figures 9 (a-e) with the aim of further study of the effects of monomer composition on terpolymer morphology. Polymer solution samples of 0.2 wt.% concentration were frozen by liquid nitrogen and then freeze-dried before SEM investigation. Figure 9a shows the SEM image of polyacrylamide (PAM) where an obvious rod-like structure was observed. The incorporation of DAC which has lower reactivity than acrylamide results in incomplete polymerization of DAC with acrylamide, so a porous irregular structure is noted as shown in Figure 9b. As can be observed in Figure 9c, the incorporation of anionic monomer AMPS highly changed the surface structure of the polymer, as a porous structure with some holes and caves on its surface was formed. Figure 9d and Figure 9e show the SEM images of the prepared terpolymer composite with different magnifications. A massive number of intermolecular linkages can be observed between the polymer chains, which lead to a significant increment in hydrodynamic volume and consequently improve the thickening properties of the nanocomposite. The reason for the dense intermolecular linkages is the presence of long hydrophobic fatty acid thermo-sensitive blocks that tend to form the intermolecular hydrophobic associations to form a three-dimensional network structure. The presence of functionalized silica results in the creation of hydrogen bonding, static electricity, and van der Waals forces formed in aqueous solution between the polymer molecules, which in turn result in the creation of rigid polymer structure and reversible physical association in the polymer solution along with a massive three-dimensional network structure significantly improves the polymer solution viscosity.

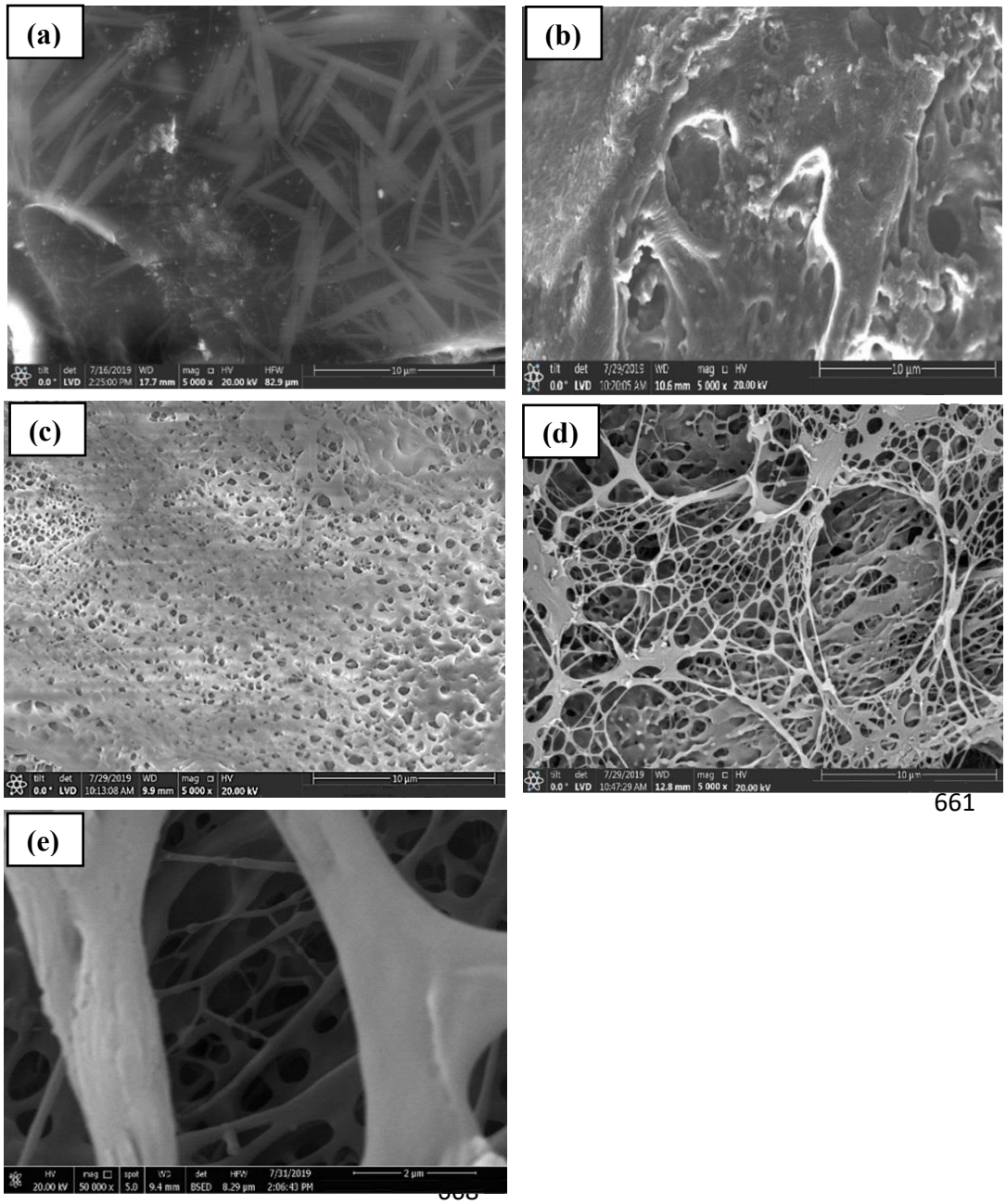

Figure 9. (a–e). SEM images of 0.2 wt.% polymer solution (a) PAM (b) P(AM/DAC) (c) P(AM/DAC/AMPS) (d) AGPC *(*e) AGPC (with different magnifications).

Energy Dispersive X-Ray (EDX) analysis of the AGPC was performed to define the elemental composition of the synthesized polymer nanocomposite and to confirm the incorporation of silica nanoparticles embedded in the nanocomposite structure. The EDX spectrum shows different intense peaks that are assigned to carbon (C) 53.77 %, oxygen (O) 33.24 %, chlorine (Cl) 0.86 %, nitrogen (N) 8.69 %, sulfur (S) 3.25 %, and silica (Si) 0.20 % atoms. The presence of Si atom peak can be easily observed. EDX spectrum in Figure 10 indicates that carbon (C) and oxygen (O) are the constituent elements of the polymer composite. The observation of C is assigned to the fatty

acid chains and O elements are assigned to esters as evident from the polymer chemical structure. Silica element is detected due to the encapsulation of silica nanoparticles in the polymer composite.

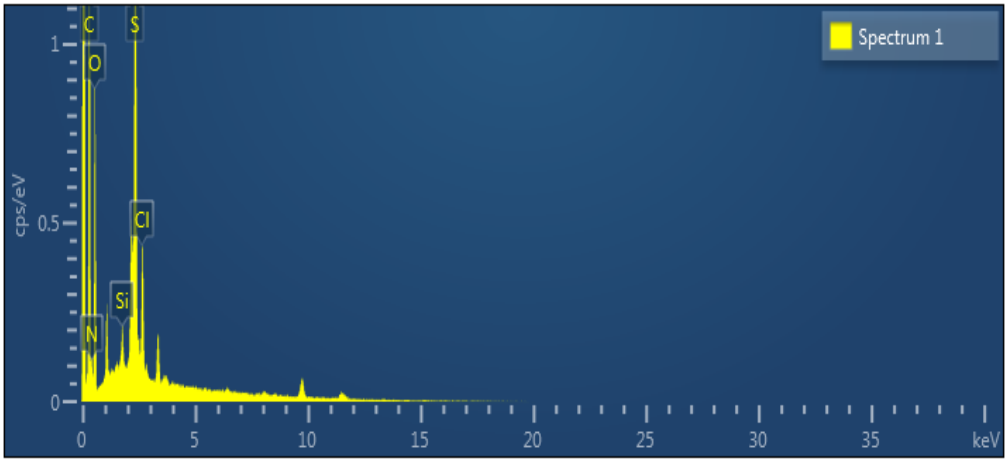

Figure 10. EDX spectra of the amphoteric green polymer composite (AGPC).

3.6 Particle size distribution and transmission electron microscopy (TEM) analysis

TEM analysis of the synthesized AGPC composite as shown in Figure 11 (a) indicates cross-linked nanosized particles owing to the enclosure of inorganic silica nanoparticles in the polymer structure. The nanoparticles are represented as dark areas inserted in the light-coloured polymer. The presence of silica nanoparticles diminishes particle aggregation which reduces the latex size. Additionally, it increases the polymer resistance against salinity and temperature. Dynamic light scattering (DLS) indicates particle size distribution varied from 33.6 to 69 nm with an average particle size of 53± 0.25 nm. Three replicates were performed to confirm data reproducibility.

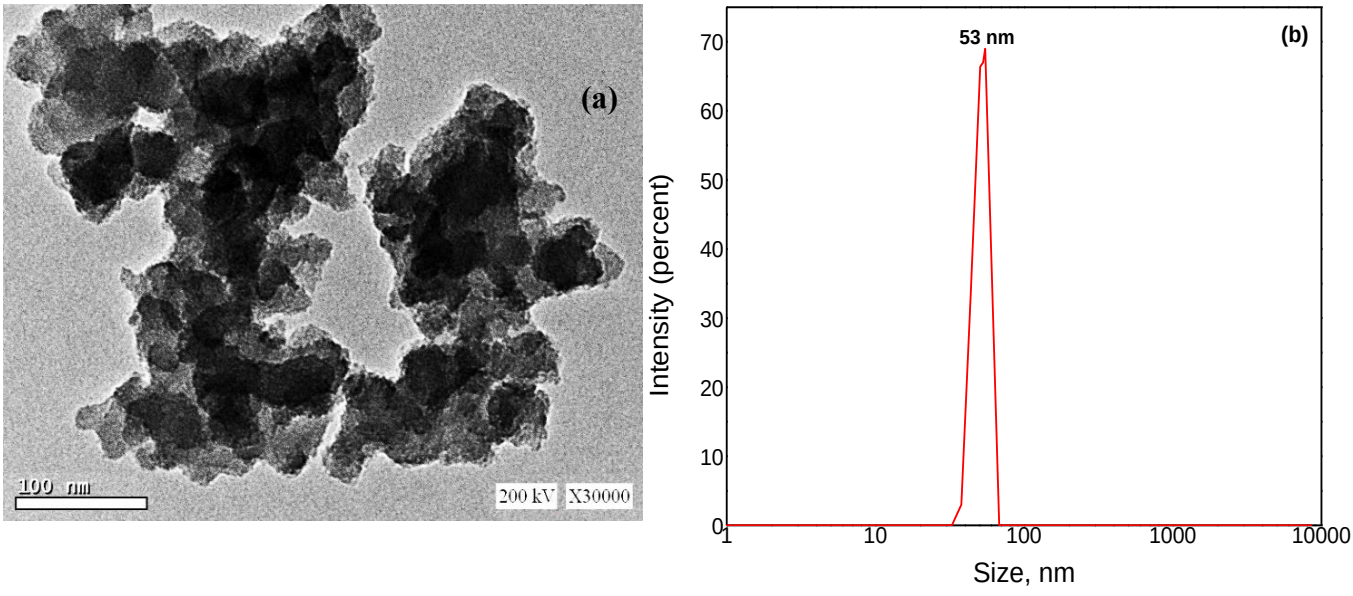

Figure 11. AGPC composite a) TEM image b) Particle size distribution: diameter of particles versus distribution %.

3.7 Mechanism of the polymerization reaction

Emulsion polymerization is initiated through the micelle nucleation mechanism by the addition of a potassium persulfate initiator (Yang et al., 2017; Fang et al., 2009). Since the applied surfactant concentration (SDS) is above the critical micelle concentration (CMC), so clusters are created. The generated free radicals are captured by SDS micelles, where monomers and initiator meet and polymerization propagation occurs (Yang et al., 2017). Termination of the polymerization process occurs after the consumption of the monomer droplets, which leads to the creation of polymer particles. The free radical polymerization reaction mechanism is indicated in Scheme 1.

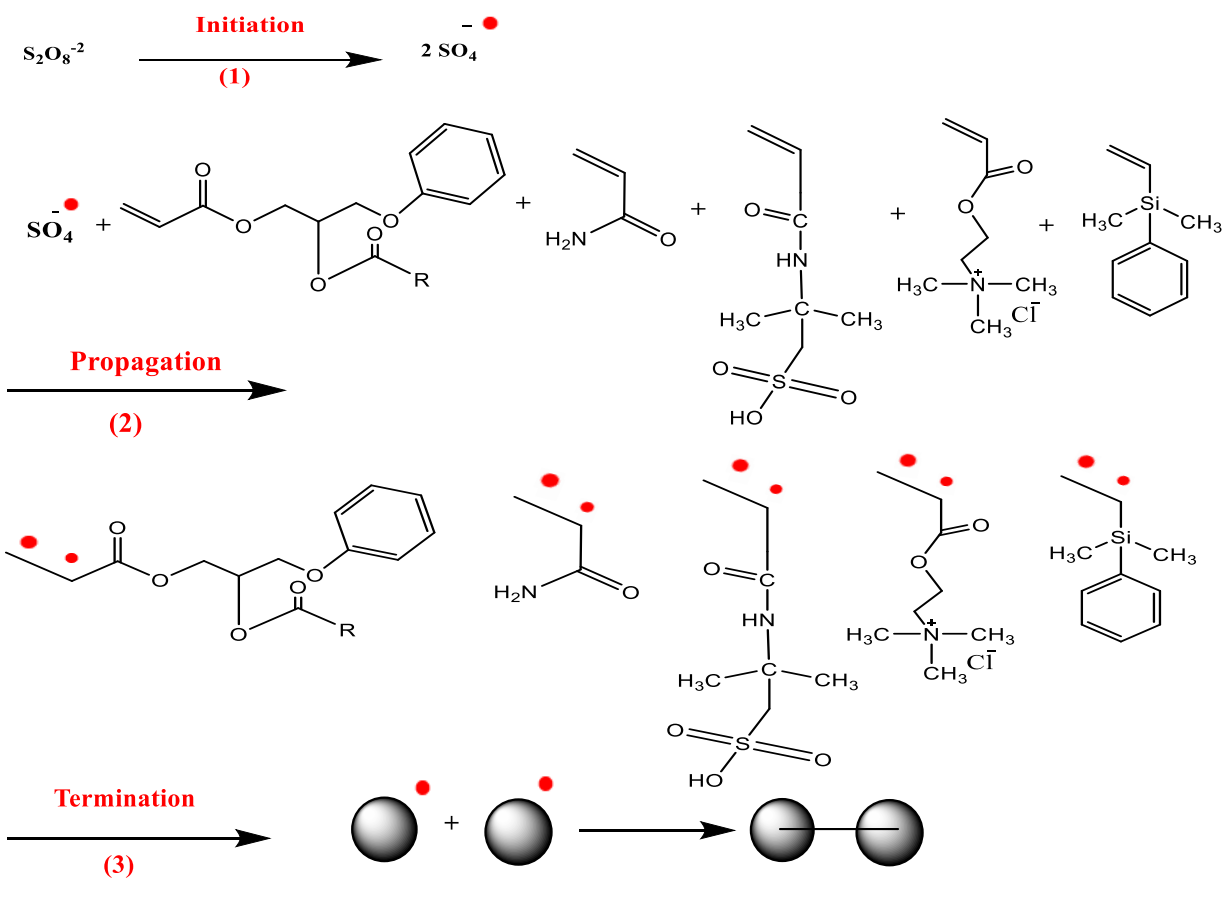

Scheme 1. Polymerization reaction mechanism of AGPC nanocomposite.

3.8 Rheological properties

The rheological properties of the synthesized polymer nanocomposite AGPC have been extensively studied. The effect of temperature, reservoir salinity, and shear rate on the apparent viscosity of AGPC polymer nanocomposite has been investigated.

3.8.1 Thermal and Ionic strength response

Unlike most of the water-soluble polymers such as HPAM which follow the Arrhenius law and show thermo-thinning behaviour either in pure water or saline environment with increasing temperature (Yang, 2001), AGPC aqueous solution exhibits unique rheological properties of

thermo-thickening behaviour that observed even at a salt-free polymer solution as well as saline environment up to 230,000 ppm at high temperatures. Figure 12 (a-d) shows the effect of salinity on different concentrations (0.15, 0.2, 0.3 and 0.4 wt.%) of AGPC aqueous solutions between 25 °C and 100 °C. As indicated in Figure 12, AGPC aqueous solutions exhibit an obvious thermoviscofying behaviour with increasing temperatures. The apparent viscosity values initially decrease with temperature, then remains almost steady, and finally increase when the critical association temperature (T_{ass}) is reached. The thermoviscofying behaviour of AGPC solutions is attributed to the formation of hydrophobic aggregations included in the OPA monomer that contributes to the creation of the 3D network and this consequently results in the increase of viscosity at high temperatures (L'alloret et al., 1997). It is also worth noting that the thermoviscofying behaviour of AGPC solution becomes more pronounced as the salinity of the aqueous solutions increased above 10,000 ppm. The value of (T_{ass}) decreases as the salinity of the aqueous solutions increases from 10,000 ppm to 230,000 ppm. This is observed at a polymer concentration of 3,000 ppm where the value of (T_{ass}) shifted from 71±2 °C to 40±3 °C as the salinity changed from 40,000 ppm to 230,000 ppm. These results are superior compared with HPAM which shows a significant reduction in viscosity with increasing temperature either in pure water or at different brine concentrations as reported by other researchers (Gou et al., 2015). This unique behaviour of AGPC can be justified by the hydrophobic effect of the "structure makers" ions that exist in the prepared synthetic water. On the one hand, this hydrophobic effect contracts the AGPC coils, which subsequently results in an abrupt decrease of apparent viscosity when adding a low salt concentration of 5,000 ppm and 10,000 ppm. On the other hand, this effect strengthens the hydrophobic fatty acid aggregation that exists in OPA monomer, which promotes the creation of a network structure in an aqueous solution and consequently increases the polymer solution viscosity (Wang et al., 2009; Liu et al., 2004; Moghaddam, 2017). The nearly unchanged viscosity over different temperature ranges might be due to the balanced effect of the two opposite behaviours. When the effect of the hydrophobic aggregations is more pronouncedly observed at high temperatures, an increase in viscosity was observed.

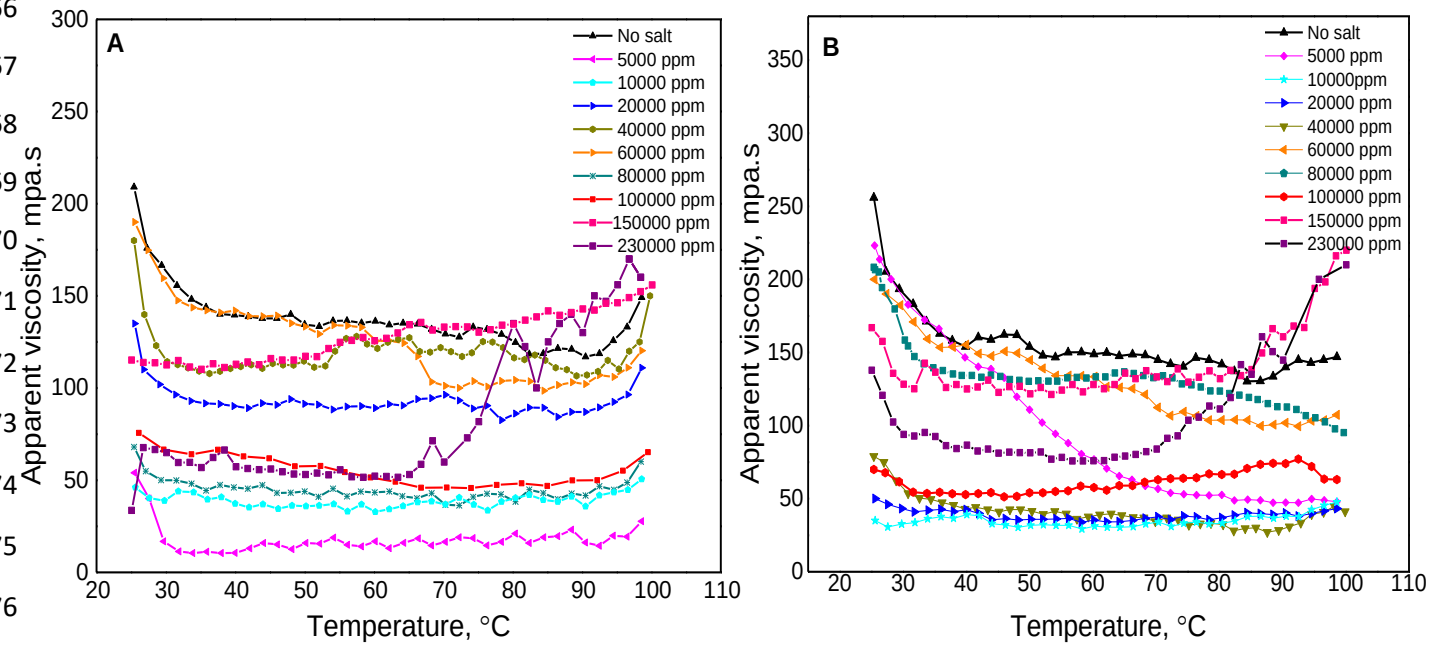

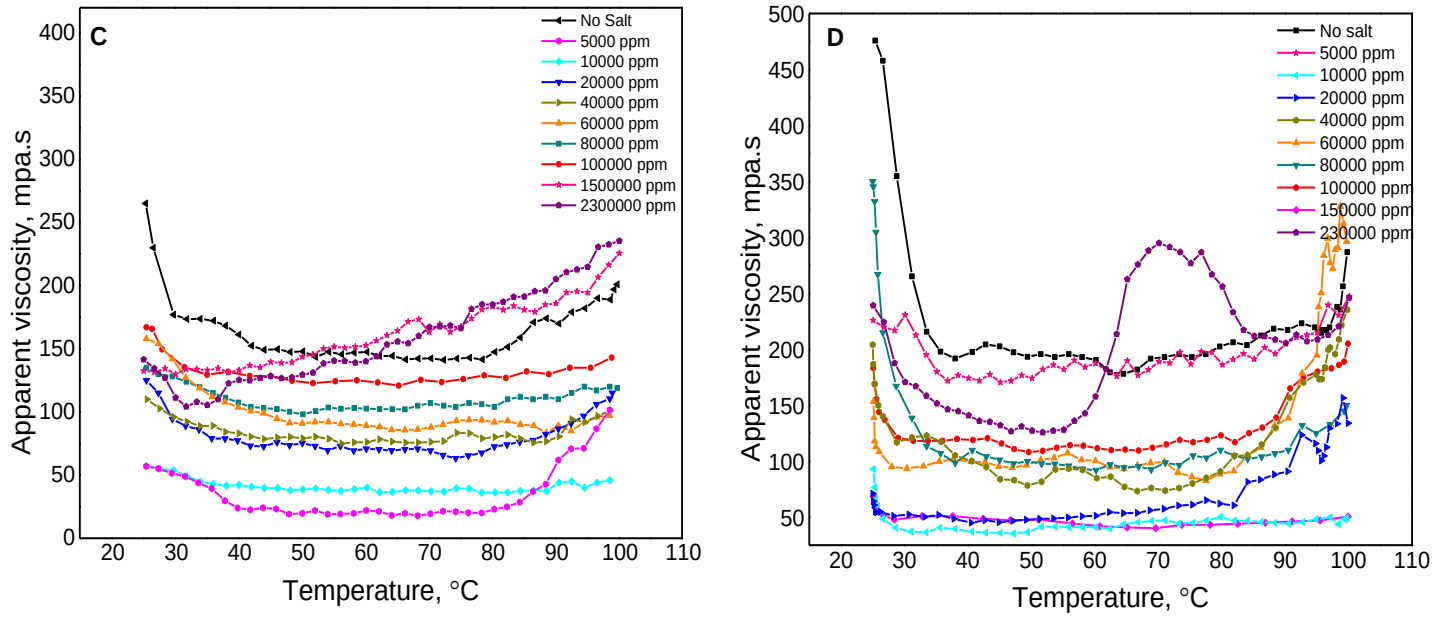

Figure 12. Apparent viscosity versus temperature for AGPC solution in different saline solution concentrations at 7.34 s^{-1} (a) C_p = 0.15 wt.% (b) C_p = 0.2 wt.% (c) C_p = 0.3 wt.% (d) C_p = 0.4 wt. %.

Figure 13 shows the apparent viscosity response of different AGPC concentrations (0.04, 0.06, 0.1, 0.5 and 0.8 wt.%) with temperature in 150,000 ppm and 230,000 ppm saline synthetic water. Many researchers reported that TVP polymers follow the Arrhenius law and exhibit a decrease of viscosity with the increase of temperature at low polymer concentrations, as high polymer concentration is always required to attain thermoviscofying behaviour. In this work, a clear thermo-thickening behaviour can be observed along with all the investigated AGPC concentrations even at ultra-low AGPC concentration of 0.04 wt.% as indicated in Figure 13. The behaviour can be attributed to the hydrophobic aggregation effect of extremely long fatty acid chains contained in OPA thermoresponsive monomer which ease viscofying properties and thermo-thickening behaviour at low polymer concentrations of 0.04, 0.06, and 0.1 wt.%. Hydrophobic aggregation is the dominant effect on the viscosity of AGPC solutions, yet minor hydrolysis may happen due to the increase in temperature as indicated in Figure S2 in the supporting information. T_{ass} decreases with increasing polymer concentration. For instance, at 230,000 ppm saline solution (Figure 13b), T_{ass} dropped from 89±1 °C to 40±3 °C as the polymer concentration changed from 0.04 wt.% to 0.8 wt.%. As the thermoviscofying property of AGPC solutions is attributed to the number of fatty acid hydrophobic aggregation which normally increases with increasing polymer concentration which significantly increases the number of the formed hydrophobic fatty acid microdomain highly increases. Accordingly, the thermoviscofying behaviour of AGPC solutions will be significantly improved and the T_{ass} value decreases with increasing polymer concentration.

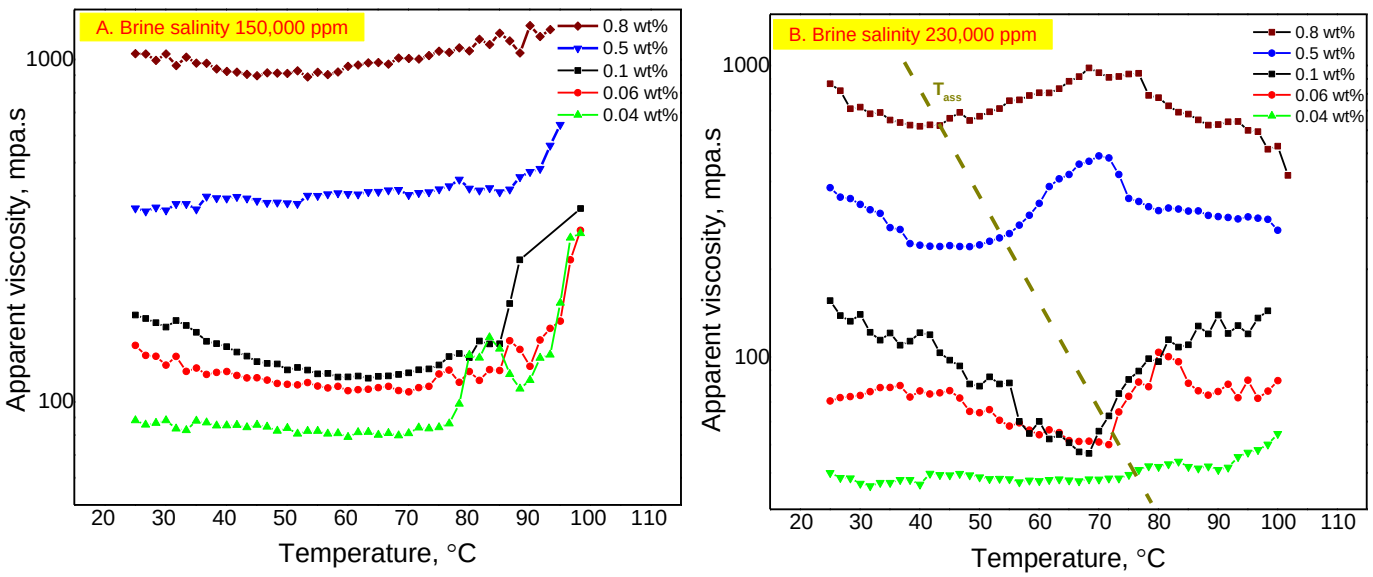

Figure 13. Apparent viscosity as a function of temperature for different polymer concentrations (C_p) of AGPC solution in synthetic brines of (a) 150,000 ppm (b) 230,000 ppm at γ= 7.34 s^{-1}.

2.8.2 Shear behaviour

The shear performance of the nanocomposite polymer solution with different AGPC solution concentrations of (0.1-0.4 wt.%) was investigated at 25 °C and, shear rates from (1.32–60 s^{-1}) as shown in Figure 14. It was observed that the apparent viscosity gradually decreases with increasing shear rates then it became almost constant with further increments in shear rate values, displaying a shear thinning behaviour. The behaviour can resort to the presence of intermolecular/intramolecular hydrogen bonding and hydrophobic associating behaviour between intra/intermolcular aggregation. In addition, the introduction of the long fatty acid hydrophobic chains of the OPA thermoresponsive monomer into the backbone structure nanocomposite improved its rheological properties. The incorporation of silica nanoparticles in the nanocomposite improved its resistance to shear. It can also be observed that higher nanocomposite concentrations displaying higher dependence of apparent viscosity on the applied shear rate. The behaviour was attributed to the presence of a higher number of polymer molecules at high composite concentrations, which result in stronger hydrophobic interactions and fatty acid chains associations (Mungan, 1970). Similarly, the shear behaviour of different AGPC concentrations (0.1-0.4 wt.%) was evaluated at a salt concentration (100,000 ppm) and temperatures of 25 °C and 100 °C, as shown in Figure 15. It is worth noting that as the temperature increased, shear viscosities of AGPC aqueous solutions show similar shear behaviour at all concentrations. It is also obvious that as the shear rate increased, AGPC solutions exhibit shear-thinning behaviour in the presence of salt at 25 °C and 100 °C. The shear thinning behavior is due to the alignment of the macromolecules along the streamline of the flow.

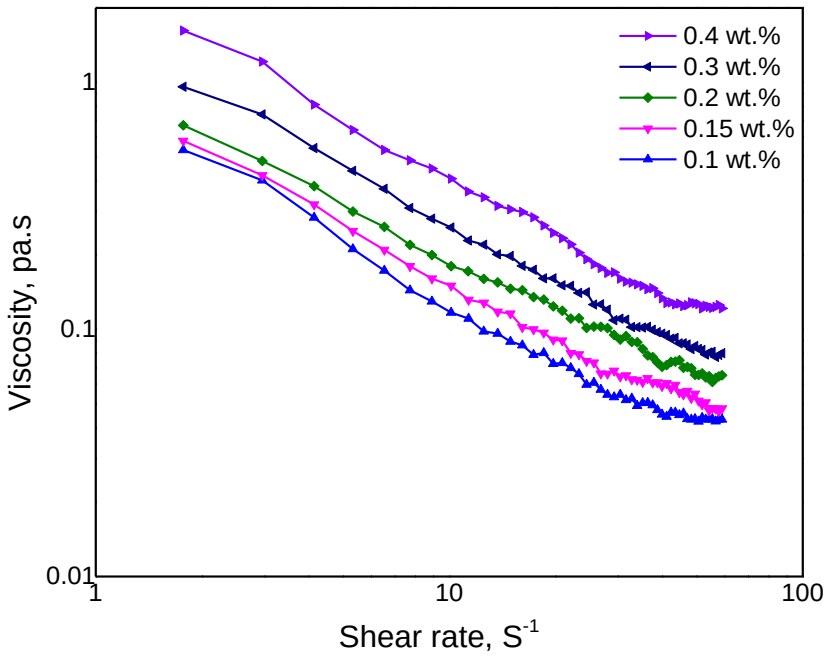

Figure 14. Apparent viscosity as a function of shear rate for AGPC solution in pure water.

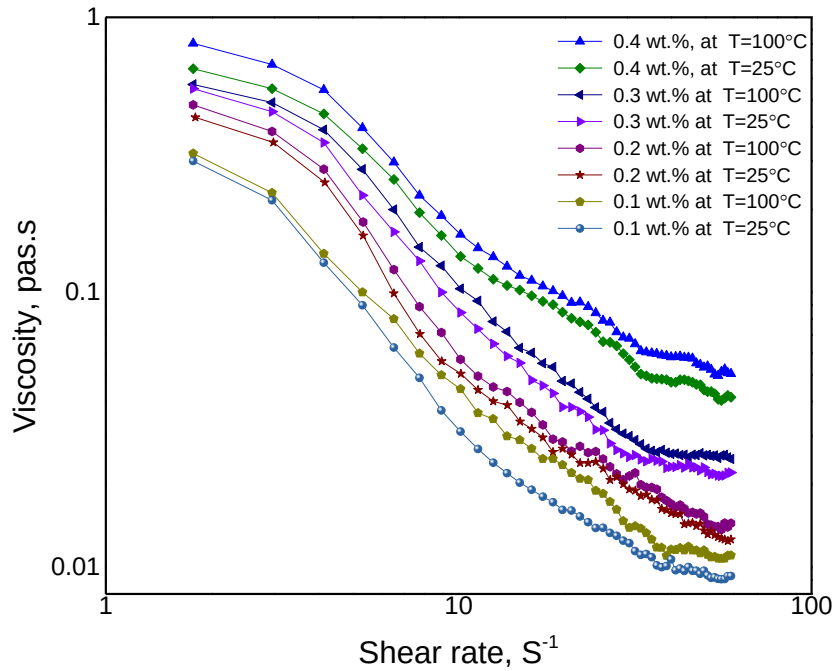

Figure 15. Apparent viscosity as a function of shear rate for AGPC solution in (100,000 ppm) saline solution at (T 25 ºC and 100 ºC).

Figure 16 shows the shear stress as a function of shear rates for nanocomposite solution concentrations of (0.1-0.4 wt.%). It is obvious that the synthesized nanocomposite exhibits shear thinning behaviour with the increase of shear rate showing a typical pseudoplastic fluid behaviour of a non-Newtonian fluid that is required for polymer flooding application (Zhang et al., 2006). That is why it can be considered as a promising polymer flooding agent for EOR application, as it will minimize the required pumping action at the wellhead. The behaviour is attributed to the gradual dissociation of molecular entanglement at a high shear rate (Zhao et al., 2015; El-Hoshoudy et al., 2018). Power-law model related shear stress (Γ; Pa) with shear rate (γ;s^{-1}) is as follows (Soliman et al., 2020):

$$\Gamma = K\gamma^{n} \quad (1)$$

Where, (k) is the coefficient of flow consistency (Pa·s^{-n}) and (n) is the flow behaviour index (Chen, 2016). In pseudoplastic behaviour, n is less than or equal to unity. Results shown in Figure 16 indicate that the estimated n values for the nanocomposite concentrations after curve fitting ranges from (0.26-0.35). This suggested that the prepared composite has a good capability of retaining the viscosity and robust pseudoplastic behaviour (Zhang et al., 2006).

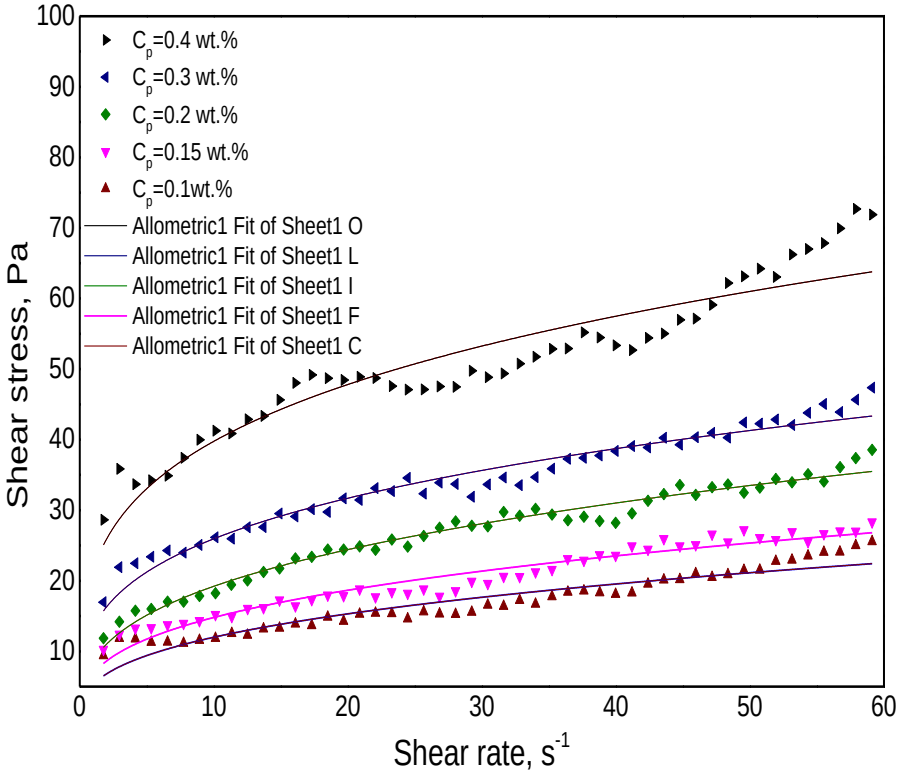

Model	Allometric1		
Equation	y=k*x^n		
Reduced Chi-	13.73611		
Adj. R-Square	0.9		
		Value	Standard Err
O	k	21.551	1.23019
	n	0.2659	0.0163

Model	Allometric1		
Equation	y=k*x^n		
Reduced Chi-	2.32901		
Adj. R-Square	0.9549		
		Value	Standard Err
L	k	13.344	0.48142
	n	0.2887	0.01026

Model	Allometric1		
Equation	y=k*x^n		
Reduced Chi-Sq	1.20704		
Adj. R-Square	0.9722		
		Value	Standard Erro
I	k	8.6756	0.30441
	n	0.3453	0.00988

Model	Allometric1		
Equation	y=k*x^n		
Reduced Chi-	1.49937		
Adj. R-Square	0.9369		
		Value	Standard Err
F	k	6.8488	0.34797
	n	0.3345	0.01434

Model	Allometric1		
Equation	y=k*x^n		
Reduced Chi-	2.20805		
Adj. R-Square	0.91		
		Value	Standard Er
C	k	5.335	0.40547
	n	0.351	0.02139

Figure 16: Shear rate as a function of shear stress for AGPC solution in pure water.

3.9 Core flooding experiments and recovery estimation

The rheological properties discussed above indicate that AGPC composite displays high thickening properties at extremely harsh reservoir conditions up to 230,000 ppm and at 100 ºC. Besides, its capability to maintain good viscosity at high shear values. Despite the unique properties of AGPC solution displaying in harsh reservoir conditions, it is crucial to evaluate its flow properties. Table 7 summarizes the pressure differential profiles, R_f and R_{rf} of the AGPC nanocomposite. Results indicated the capability of AGPC solutions to build R_f throughout polymer flooding even at low polymer concentrations. The high values of R_f factors are assigned to 1) the thermoviscofying behaviour of AGPC due to the creation of hydrophobic aggregations of thermo-sensitive blocks included OPA monomer which results in the creation of a 3D network and increasing solution viscosity at high temperature and high salinity this consequently slowed down the composite flow in the porous media and increased the differential pressure and the resulted resistance factors (Grattoni et al., 2004); 2) the presence of SiO_2 particles which forms three-dimensional network structure and adsorbed on the rock surface forming boundary layer which consequently increases the permeation resistance force and improves sweep efficiency (Chang et al., 2000; Hunter et al., 2008). Accordingly, the application of AGPC nanocomposite would pronouncedly improve mobility ratio and water injection profile. High R_{rf} values (5.77−11.6) implied lower permeability, which subsequently improves displacement efficiency. As indicated in Table 7, after flooding of the three AGPC concentrations, ζ / r_p values were less than 50 % signifying that more than half the pore spaces of the cores are open for fluid flow after adsorption (Zaitoun and Kohler, 1988). The ζ / r_p value of AGPC concentration of 0.1 wt.% was greater than that of 0.06 wt.% by 1.49 % and greater than that of 0.04 wt.% concentrations by 8.38 %, suggesting higher permeability reduction which results in higher R_{rf}. The reported thickness of the absorbed nanocomposite layer ranges from 1.52-1.96 μm, which is a thin layer thickness that will not adversely affect core permeability.

Table 7: Pressure differential profiles, R_f and R_{rf} of the polymer composite evaluated at 230,000 ppm and 100 °C.

Core sample	C_P wt.%	ΔP_p bar	ΔP_w bar	ΔP_{wp} bar	K_w mD	K_{wp} mD	R_f	R_{rf}	r μm	ζ μm	ζ / r_p (%)
Core#1	0.04	1.154	0.2	0.88	521.53	139.07	5.77	4.4	4.92	1.52	30.89
Core#2	0.06	1.69	0.2	1.344	511.10	77.18	8.45	6.72	4.87	1.84	37.78
Core#3	0.1	2.09	0.18	1.42	537.10	70.18	11.61	7.88	4.99	1.96	39.27

Accordingly, three cores with approximate brine permeability were used in core flooding experiments to measure the incremental oil recovery driven by AGPC nanocomposite using the core flooding setup shown in Figure 2. Different concentrations 0.04 wt.%, 0.06 wt.% and 0.1 wt. % of AGPC nanocomposite solutions were applied in displacement tests. Recovered oil production and flooding pressure drop were reported as a function of injected pore volume for each nanocomposite concentration as shown in Figure 17. As indicated in Figure 17 and Table 8, AGPC nanocomposite solutions can increase oil recovery factor by 15.4±0.1 % using AGPC

concentrations of 0.04 wt.%, 22.6±0.3 % using AGPC concentrations of 0.06 wt.% and 25±0.2 % using AGPC concentrations of 0.1 wt.%. Figure 17 indicates the pressure drop across the cores during injection of the AGPC concentrations. It is notable that the pressure drop was almost steady during the injection of brine. When AGPC solution was injected the pressure drop initially increased with the injected pore volume and then stabilizes. The higher the AGPC concentration, the more injected pore volume was needed to reach the pressure drop stabilization which signifies the capability of AGPC solutions to delay water breakthrough with increasing its injected concentration. The increase of pressure drop can be attributed to temporary log-jamming triggered by aggregation of nanosized AGPC particles at the pore throats along with high R_f throughout the core due to increased AGPC solution viscosity at HSHT flooding conditions. The higher the concentration of AGPC nanocomposite, the higher the AGPC solution viscosity which increases the pressure differential. This explains the increase of oil recovery with increasing the injected AGPC concentration as maximum oil recovery was achieved at AGPC concentration of 0.1 wt.% with a total cumulative oil recovery of 70 % and tertiary oil recovery of 25 %. This is also justifying the abrupt increment in oil recovery for AGPC concentration of 0.1 wt.% at 0.2 injected pore volume where the increase of AGPC solution viscosity is more substantial at higher AGPC concentrations. The results are in good agreement with the published literature (Pu et al., 2018).

Table 8 summarizes the cumulative oil recovery results of the three nanocomposite concentrations. The reported oil recovery by AGPC solutions is higher than TVP polymer alternatives as indicated in Table 9. For instance, as observed in Table 9, the TVP polymer evaluated by (Kamal et al., 2015b) achieved an oil recovery of 22 % by using polymer concentration of 0.25 wt.% and 0.05 wt.% surfactant, while 25 % oil recovery was achieved by applying only 0.1 wt.% of AGPC solution that demonstrates higher efficiency and economical visibility of AGPC nanocomposite. The reasonable capability of the novel AGPC nanocomposite solutions to increase oil recovery factor compared to that of HPAM can be attributed to (1) thermoviscofying properties along with amphoteric nature of the AGPC nanocomposite which results in high solution viscosity at high salinity and temperature conditions; (2) the thickening properties of the supramolecular structure created by the incorporation of the long fatty acid hydrophobic chains of the thermoresponsive monomer OPA, which consequently increases the molecule hydrodynamic volume which decreases the mobility ratio and improves displacement efficiency; (3) The presence of SiO_2 nanoparticles enhances the solution viscosity during flooding due to the created 3D-molecular network structure *via* H-bonding, static electricity and van der Waals forces formed in aqueous solution between the polymer molecules. The capability of AGPC nanoparticles to behave as wetting agent at small pore throats and peels off the oil film that attached to the rock surface which increases the volume of recovered oil. This mechanism was proved by (Chang et al., 2000; Hunter et al., 2008; Pu et al., 2018).

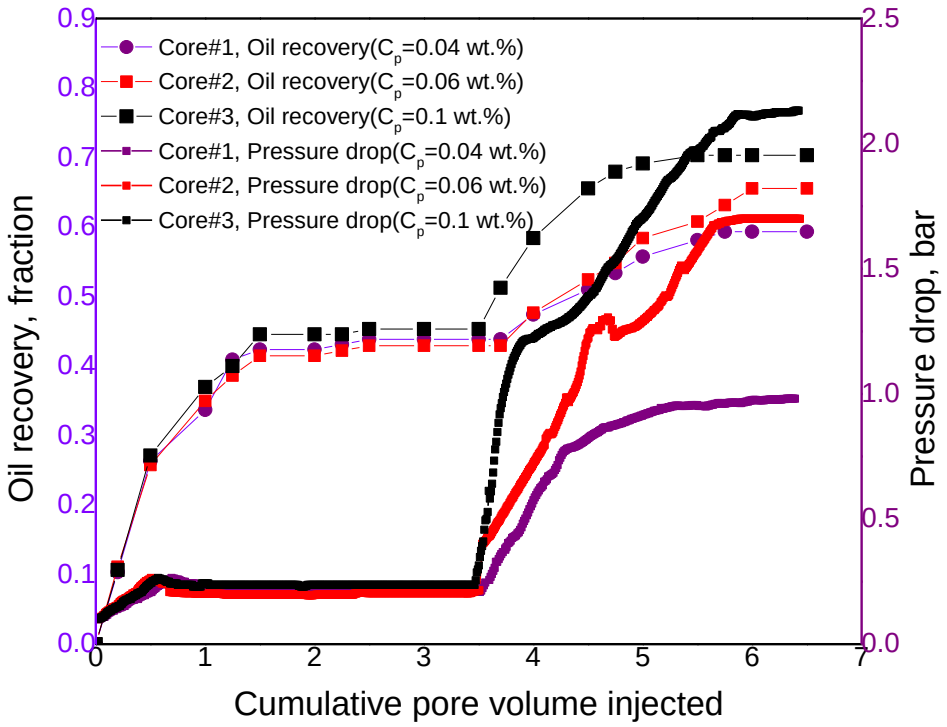

Figure 17: Cumulative oil recovery and flooding pressure as a function of injected pore volume for different AGPC concentrations.

Table 8. Summary of oil recovery results of AGPC nanocomposite.

Core	Polymer concentration (C_p)	Volume of oil injected (V_{oi})	Volume of water remain (V_{wc})	Saturation		Water flooding recovery (E_w)	Polymer flooding recovery (E_p)
	wt. %	cc	cc	%PV		%	%
				Initial oil saturation (S_{oi}), %	Residual oil saturation (S_{or}), %		
Core#1	0.04±0.0001	8.4	3.01	73.6±0.1	41.2±0.11	44.0±0.1	15.4±0.1
Core#2	0.06±0.0001	8.2	2.9	73.8±0.1	42.3±0.11	42.6±0.12	22.6±0.3
Core#3	0.1±0.0001	8.6	3.3	72.2±0.1	39.4±0.14	45.3±0.16	25±0.2

Table 9. Comparison between the additional oil recovery reported by previous studies and the current study.

Published works	Flooding Concentration, wt. %	Additional oil recovery, %
Tamsilian et al. (Tamsilian et al., 2020)	0.2	7.03
Kamal et al. (Kamal et al., 2015b)	0.25+0.05 % surfactant	22
Chen et al. (Chen et al., 2013)	0.2	13.5
Li et al. (Li et al., 2017a)	0.2	15.5
Current study	0.1	25

3.10 Evaluation of sandstone rock wettability

In EOR, wettability has a crucial influence as water-wet rock surfaces enhance the efficiency of oil displacement. In this work, the nanocomposite capability to alter the rock wettability was assessed by measuring the contact angle of oil drop on a sandstone surface immersed in AGPC solution. To get an oil-wet surface, glass sheets represent sandstone surfaces were submerged in paraffin aged for 72 h at 80 °C (Li et al., 2017b). The oil-wet glass sheet is then immersed in both brine and AGPC solutions at 60 °C for 24 hours. The contact angle between the oil droplet and the glass surface in each liquid phase were evaluated. Three replicates were performed, and the standard error was reported. As indicated in Figure 18, AGPC solution decreased the contact angle between the sandstone surface and an oil drop from 152.7 ±0.07º (in brine) to 82.95 ±0.9º, which indicate that the sandstone surface was altered to be water-wet which means the oil is less adhere on the sandstone surface. The microscopic mechanism of oil displacement by AGPC nanocomposite wettability alteration is indicated in Figure 19. The sandstone surface is negatively charged owing to the presence of negatively charged oxygen atoms attached with silicates. The positively charged sodium cations from salt water attracted to negatively charged silicates making a positive charge on the sandstone surface. The negatively charged carboxyl group -COOH of crude oil, which mainly exists in its heavy end fractions, forms a strong bond with positively charged sodium cations. As a result, the sandstone surface gets covered with crude oil molecules and the wettability of sandstone surface changed to oil wet (Derkani et al., 2018)(Figure 19a). The GC hydrocarbon profile is indicated in the supporting information in Figure S3 and the detailed composition of the crude oil is summarized in Table S1. The carboxylic group exist in the crude oil was determined using acid number (AN). The crude oil used in this research has AN 0.041 mg KOH/g. The main mechanism for oil curling by AGPC nanocomposite is the adsorption of AGPC where its charged moieties interact with sandstone in the presence of salt-water cations *via* ionic exchange to improve oil recovery. As indicated in Figure 19(b and c), the positively charged quaternary amine of AGPC interacts with sandstone silicates. The AGPC anions (sulfonate group) were then moved to the external sandstone surface to interact with sodium cations of salt water which increases the negative charges of the sandstone surface and alter the sandstone surface to more water wet state liberating the crude oil from the sandstone surface (Derkani et al., 2018; Abdullah et al., 2017; Elsaeed et al., 2021). The presence of silica nanoparticles in the polymer chain makes the AGPC nanocomposite behaves as a wetting agent at extremely small contact angles which improves the displacement of oil leaving the sandstone surface water wet (McElfresh

et al., 2012; Zhao and Pu, 2020; Zhao et al., 2019) which is proved by reduced contact angle to approximately 83 º.

a) **b)**

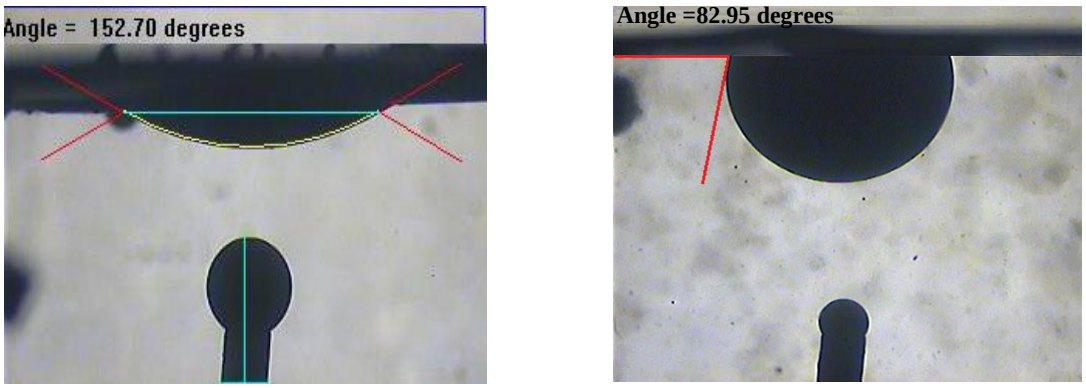

Figure 18: Crude oil drop on sandstone surface immersed in (a) 230,000 ppm brine and (b) AGPC solution.

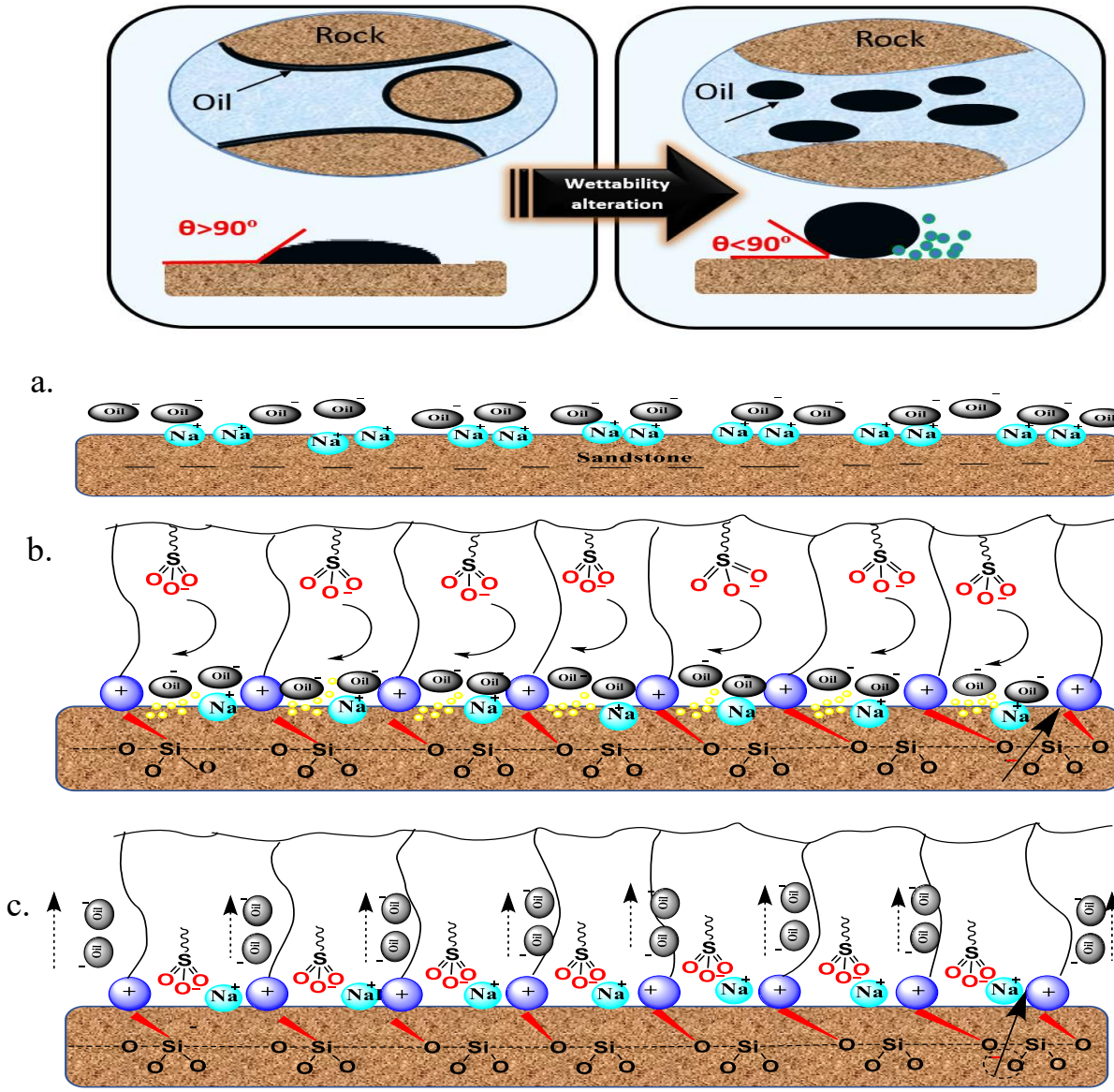

Figure 19. Proposed mechanism of crude oil displacement by AGPC solution.

3.11 Conclusions

A green transesterification reaction route was utilized to synthesize a novel OPA thermosensitive monomer derived from WVO, which was then grafted on poly(acrylamide/2-acrylamido-2-methyl-1-propanesulfonic acid/acrylacyloxyethyltrimethyl ammonium chloride) terpolymer through free radical polymerization in the presence of dimethylphenylvinylsilane derivative to synthesize a novel high molecular weight thermo-responsive nanocomposite for EOR application at hostile reservoir conditions. The chemical structures of the synthesized OPA monomer and AGPC nanocomposite were characterized by FT-IR and ^{1}H NMR techniques. The properties of AGPC nanocomposite were then intensively investigated by TGA, SEM, EDX, TEM, DLS and

GPC characterization techniques. Based on the experimental results, the following conclusions can be drawn:

- The synthesized AGPC nanocomposite showed conspicuous thermoviscofying behaviour and superior thickening performance in extreme saline environments up to 230,000 ppm even at ultra-low nanocomposite concentrations of 0.04 wt.% as well as salt-free solutions.
- Exhibit high resistance factor (R_f) value of 11.61 and residual resistance factor (R_{rf}) value of 7.88 at a low polymer concentration of 0.1 wt.%, which proves its ability to improve the sweeping efficiency.
- Excellent capability to provide high oil recovery of 25±0.2 % of residual oil saturation (% S_{or}) using low polymer concentration of 0.1 wt.% at extremely harsh reservoir conditions of 230,000 ppm and at 100 ºC, which is more efficient with higher economic benefit than applying other abovementioned TVP polymers.
- The novel nanocomposite showed a promising result to change the wettability of sandstone rock surface from oil-wet rock to water-wet, which increases oil recovery.
- This is the first study of the adaptation of WVO into a high value thermo-sensitive nanocomposite for EOR application at extremely harsh reservoir conditions of total dissolved solids (TDS) of 230,000 ppm and at 100 ˚C.

Acknowledgement

The authors acknowledge The British University in Egypt (BUE) and London South Bank University (LSBU) for supporting this research.

Declarations of interest

None.

Authors Contributions

Shahenda Mahran (PhD student): Conceptualization, materials synthesis and characterization, methodology, performed all experiments in the laboratory, results interpretation, formal analysis, writing - original draft; Attia Attia: Conceptualization, supervision, project administration, resources, funding acquisition; Basudeb Saha: Conceptualization, writing review and editing, formal analysis, resources, supervision, project administration, funding acquisition.

References

Abdullah, M., Alquraishi, A., Allohedan, H. A., Almansour, A. O. and Atta, A. M. 2017. Synthesis of novel water soluble poly (ionic liquids) based on quaternary ammonium acrylamidomethyl propane sulfonate for enhanced oil recovery. Journal of Molecular Liquids, 233, 508-516.

Aboelazayem, O., El-gendy, N. S., Abdel-rehim, A. A., Ashour, F. and Sadek, M., 2018. Biodiesel production from castor oil in egypt: process optimisation, kinetic study, diesel engine performance and exhaust emissions analysis. Energy, 157, 843-852.

Aboelazayem, O., Gadalla, M., Alhajri, I. and Saha, B., 2021. Advanced process integration for supercritical production of biodiesel: Residual waste heat recovery via organic Rankine cycle (ORC). Renewable Energy, 164, 433-443.

Dekunle, k., Akesson, D. and Skrifvars, M., 2010. Biobased composites prepared by compression molding with a novel thermoset resin from soybean oil and a natural-fiber reinforcement. Journal of Applied Polymer Science, 116, 1759-1765.

Akbari, S., Mahmood, S. M., Ghaedi, H. and AL-HAJRI, S. 2019. A new empirical model for viscosity of sulfonated polyacrylamide polymers. Polymers, 11, 1046.

Akbari, S., Mahmood, S. M., Tan, I. M., Ghaedi, H. and Ling, O. L. 2017a. Assessment of polyacrylamide based co-polymers enhanced by functional group modifications with regards to salinity and hardness. Polymers, 9, 647.

Akbari, S., Mahmood, S. M., Tan, I. M., Ling, O. L. and Ghaedi, H. 2017b. Effect of aging, antioxidant, and mono-and divalent ions at high temperature on the rheology of new polyacrylamide-based co-polymers. Polymers, 9, 480.

Al-degs, Y. S., Al-ghouti, M. and Salem, N., 2011. Determination of frying quality of vegetable oils used for preparing falafel using infrared spectroscopy and multivariate calibration. Food Analytical Methods, 4, 540-549.

Alramahi, B. A., Alshibli, K. A. and Attia, A. M., 2005. Influence of grain size and consolidation pressure on porosity of rocks. Site Characterization and Modeling, 1-3.

Alshibli, K. A., Alramahi, B. A. and Attia, A. M., 2006. Assessment of spatial distribution of porosity in synthetic quartz cores using microfocus computed tomography (μct). Particulate Science and Technology, 24, 369-380.

Bastiat, G., Grassl, B. and François, J., 2002. Study of sodium dodecyl sulfate/poly (propylene oxide) methacrylate mixed micelles for the synthesis of thermo-associative polymers by micellar polymerization. Polymer International, 51, 958-965.

Chang, T., Wang, Y., Hong, Y. and Chiu, Y., 2000. Organic–inorganic hybrid materials. V. dynamics and degradation of poly (methyl methacrylate) silica hybrids. Journal of polymer science Part A: Polymer Chemistry, 38, 1972-1980.

Chen, Q., Wang, Y., Lu, Z. and Feng, Y., 2013. Thermoviscosifying polymer used for enhanced oil recovery: rheological behaviors and core flooding test. polymer bulletin, 70, 391-401.

Chen, Z., 2016. Polyacrylamide and its derivatives for oil recovery. Doctoral dissertation, Missouri University of Science and Technology.

Chuang, C.-K., Yeung, C.-Y., Jim, W.-T., Lin, S.-P., Wang, T.-J., Huang, S.-F. and Liu, H.-L. 2013. Comparison of free fatty acid content of human milk from Taiwanese mothers and infant formula. Taiwanese Journal of Obstetrics and Gynecology, 52, 527-533.

Derkani, M. H., Fletcher, A. J., Abdallah, W., Sauerer, B., Anderson, J. and Zhang, Z. J. 2018. Low salinity waterflooding in carbonate reservoirs: Review of interfacial mechanisms. Colloids and Interfaces, 2, 20.

Donaldson, E. C., Chilingarian, G. V. and Yen, T. F., 1989. Enhanced oil recovery, ii: Processes and operations, Elsevier,USA.

Dudley, B., 2019. BP statistical review of world energy. BP statistical review, London, UK, Accessed Aug, 6, 2019.

Durand, A. and Hourdet, D., 1999. Synthesis and thermoassociative properties in aqueous solution of graft copolymers containing poly (n-isopropylacrylamide) side chains. Polymer, 40, 4941-4951.

Durand, A. and Hourdet, D., 2000. Thermoassociative graft copolymers based on poly (n-isopropylacrylamide): Effect of added co-solutes on the rheological behaviour. Polymer, 41, 545-557.

El-hoshoudy, A., Desouky, S. and Attia, A., 2018. Synthesis of starch functionalized sulfonic acid co-imidazolium/silica composite for improving oil recovery through chemical flooding technologies. International Journal of Biological Macromolecules, 118, 1614-1626.

Elsaeed, S. M., Zaki, E. G., Omar, W. A., Ashraf Soliman, A. and Attia, A. M. 2021. Guar Gum-Based Hydrogels as Potent Green Polymers for Enhanced Oil Recovery in High-Salinity Reservoirs. ACS omega, 6, 23421-23431.

Fang, Y., Yu, H., Chen, l. and Chen, S., 2009. Facile glycerol-assisted synthesis of n-vinyl pyrrolidinone-based thermosensitive hydrogels via frontal polymerization. Chemistry of Materials, 21, 4711-4718.

Fernandes, F. C., Kirwan, K., Wilson, P. R. and Coles, S. R., 2019. Sustainable alternative composites using waste vegetable oil based resins. Journal of Polymers and the Environment, 27, 2464-2477.

Gou, S., He, Y., Ma, Y., Luo, S., Zhang, Q., Jing, D. and Guo, Q., 2015. A water-soluble antimicrobial acrylamide copolymer containing sulfitobetaine for enhanced oil recovery. RSC Advances, 5, 51549-51558.

Grattoni, C., Luckham, P., Jing, X., Morman, l. and Zimmerman, R. W., 2004. Polymers as relative permeability modifiers: adsorption and the dynamic formation of thick polyacrylamide layers. Journal of Petroleum Science and Engineering, 45, 233-245.

Gunstone, F. D., 2012. Fatty acid and lipid chemistry, Springer, US, 2012.

Hayakawa, S. and Hench, I. I., 2000. AM1 study on infra-red spectra of silica clusters modified by fluorine. Journal of Non-Crystalline Solids, 262, 264-270.

Hourdet, D., L'alloret, F. and Audebert, R., 1994. Reversible thermothickening of aqueous polymer solutions. Polymer, 35, 2624-2630.

Hunter, T. N., Pugh, R. J., Franks, G. V. and Jameson, G. J., 2008. The role of particles in stabilising foams and emulsions. Advances in Colloid and Interface Science, 137, 57-81.

Kamal, M. S., Sultan, A. S., Al-mubaiyedh, U. A., Hussein, I. A. and Feng, Y., 2015. Rheological properties of thermoviscosifying polymers in high-temperature and high-salinity environments. The Canadian Journal of Chemical Engineering, 93, 1194-1200.

Kamal, M. S., Sultan, A. S., Al-mubaiyedh, U. A., Hussein, I. A. and Feng, Y. 2015b. Rheological properties of thermoviscosifying polymers in high-temperature and high-salinity environments. The Canadian Journal of Chemical Engineering, 93, 1194-1200.

L'alloret, F., Hourdet, D. and Audebert, R., 1995. Aqueous solution behavior of new thermoassociative polymers. Colloid and Polymer Science, 273, 1163-1173.

L'alloret, F., Maroy, P., Hourdet, D. and Audebert, R., 1997. Reversible thermoassociation of water-soluble polymers. Revue de l'institut français du pétrole, 52, 117-128.

Lai, N., Wu, T., Ye, Z., Zhou, N., Xu, Q. and Zeng, F., 2016. Preparation and properties of hyperbranched polymer containing functionalized nano-SiO_2 for low-moderate permeability reservoirs. Russian Journal of Applied Chemistry, 89, 1681-1693.

Li, X. E., Xu, Z., Yin, H., Feng, Y. and Quan, H., 2017. Comparative studies on enhanced oil recovery: thermoviscosifying polymer versus polyacrylamide. Energy & Fuels, 31, 2479-2487.

Li, Y., Dai, C., Zhou, H., Wang, X., LV, W., WU, Y. and Zhao, M. 2017b. A novel nanofluid based on fluorescent carbon nanoparticles for enhanced oil recovery. Industrial & Engineering Chemistry Research, 56, 12464-12470.

Liu, R., Pu, W., Du, D., Gu, J. and Sun, L., 2018. Manipulation of star-like polymer flooding systems based on their comprehensive solution properties and flow behavior in porous media. Journal of Petroleum Science and Engineering, 164, 467-484.

Liu, X.-M., Wang, L.-S., Wang, L., Huang, J. and He, C., 2004. The effect of salt and pH on the phase-transition behaviors of temperature-sensitive copolymers based on n-isopropylacrylamide. Biomaterials, 25, 5659-5666.

Machado, T. O., Cardoso, P. B., Feuser, P. E., Sayer, C. and Araújo, P. H. 2017. Thiol-ene miniemulsion polymerization of a biobased monomer for biomedical applications. Colloids and Surfaces B: Biointerfaces, 159, 509-517.

Mahran, S., Attia, A. and Saha, B. 2018, A review on polymer flooding in enhanced oil recovery under harsh conditions. 11th international sustainable energy & environmental protection conference.

Mcelfresh, P., Wood, M. and Ector, D. Stabilizing nano particle dispersions in high salinity, high temperature downhole environments. SPE International Oilfield Nanotechnology Conference and Exhibition, 2012. OnePetro.

Moghaddam, S. Z., 2017. Specific ion effects in thermo-responsive polymer solutions. Doctoral dissertation, Technical University of Denmark.

Nesic, A. R., Panic, V. V., Onjia, A. E. and Velickovic, S. J. 2015. The enhanced removal of cationic dyes in binary system using novel copolymers with two kinds of acidic groups. Colloids and Surfaces A: Physicochemical and Engineering Aspects, 476, 24-34.

Petit, l., Karakasyan, C., Pantoustier, N. and Hourdet, D., 2007. Synthesis of graft polyacrylamide with responsive self-assembling properties in aqueous media. Polymer, 48, 7098-7112.

Pu, W., Zhao, S., Wang, S., Wei, B., Yuan, C. and Li, Y. 2018. Investigation into the migration of polymer microspheres (PMs) in porous media: Implications for profile control and oil displacement. Colloids and Surfaces A: Physicochemical and Engineering Aspects, 540, 265-275.

Quan, H., Li, Z. and Huang, Z., 2016. Self-assembly properties of a temperature-and salt-tolerant amphoteric hydrophobically associating polyacrylamide. RSC Advances, 6, 49281-49288.

Soliman, A. A., El-hoshoudy, A. N. and Attia, A. M., 2020. Assessment of xanthan gum and xanthan-g-silica derivatives as chemical flooding agents and rock wettability modifiers. Oil & Gas Science and Technology–revue d'ifp Energies nouvelles, 75, 12.

Sayyouh, M., Al-blehed, M. and Attia, A., 1993. The effect of alkaline and polymer additives on phase behaviour of surfactant-oil-brine system at high salinity conditions.Revue de l'institut Français du Pétrole, 48, 359-369.

Song, Z., Liu, L., Wei, M., Bai, B., Hou, J., Li, Z. and Hu, Y., 2015. Effect of polymer on disproportionate permeability reduction to gas and water for fractured shales. Fuel, 143, 28-37.

Su, X. and Feng, Y. 2018. Thermoviscosifying smart polymers for oil and gas production: State of the art. ChemPhysChem, 19, 1941-1955.

Suzuki, A. H., Botelho, B. G., Oliveira, L. S. and Franca, A. S., 2018. Sustainable synthesis of epoxidized waste cooking oil and its application as a plasticizer for polyvinyl chloride films. European Polymer Journal, 99, 142-149.

Tamsilian, Y., Shirazi, M., Sheng, J. J., Agirre, A., Fernandez, M. and Tomovska, R., 2020. Advanced oil recovery by high molar mass thermoassociating graft copolymers. Journal of Petroleum Science and Engineering, 192, 107290.

Tian, Q., Sun, L. H. and Kou, H. H., 2014. Study on laboratory evaluation of temperature and salt resistance polymer solution. Applied Mechanics and Materials. Trans Tech Publ, 217-221.

Umar, Y., Velasco, O., Abdelaziz, O. Y., Aboelazayem, O., Gadalla, M. A., Hulteberg, C. P. and Saha, B. 2022. A renewable lignin-derived bio-oil for boosting the oxidation stability of biodiesel. Renewable Energy, 182, 867-878.

Wang, Y.-C., Li, Y., Yang, X., Yuan, Y., Yan, L.-F. and Wang, J., 2009. Tunable thermosensitivity of biodegradable polymer micelles of poly (ε-caprolactone) and polyphosphoester block copolymers. Macromolecules, 42, 3026-3032.

Wang, Y., Feng, Y., Wang, B. and Lu, Z., 2010. A novel thermoviscosifying water-soluble polymer: synthesis and aqueous solution properties. Journal of Applied Polymer Science, 116, 3516-3524.

Wu, J., Wang, H.-F., Wang, X.-B., Yang, H.-Y., Jiang, R.-Y. and Zeng, R. J., 2017. Design and characterization of a microbial self-healing gel for enhanced oil recovery.RSC Advances, 7, 2578-2586.

Yang, H. and Irudayaraj, J., 2000. Characterization of semisolid fats and edible oils by fourier transform infrared photoacoustic spectroscopy. Journal of the American Oil Chemists' Society, 77, 291-295.

Yang, M. H., 2001. Flow behavior of polyacrylamide solution. iii. mathematical treatment. Journal of Applied Polymer Science, 82, 2784-2789.

Yang, Y., Fang, Z., Chen, X., Zhang, W., Xie, Y., Chen, Y., Liu, Z. and Yuan, W., 2017. An overview of pickering emulsions: solid-particle materials, classification, morphology, and applications. Frontiers in Pharmacology, 8, 287.

Zaitoun, A. and Kohler, N., 1988. Two-phase flow through porous media: effect of an adsorbed polymer layer. SPE Annual Technical Conference and Exhibition. Society of Petroleum Engineers.

Zhang, D. L., Liu, S., Puerto, M., Miller, C. A. and Hirasaki, G. J., 2006. Wettability alteration and spontaneous imbibition in oil-wet carbonate formations. Journal of Petroleum Science and Engineering, 52, 213-226.

Zhang, H., Zhai, D. and He, Y., 2014. Graphene oxide/polyacrylamide/carboxymethyl cellulose sodium nanocomposite hydrogel with enhanced mechanical strength: preparation, characterization and the swelling behavior. RSC Advances, 4, 44600-44609.

Zhao, S. and Pu, W. 2020. Migration and plugging of polymer microspheres (PMs) in porous media for enhanced oil recovery: Experimental studies and empirical correlations. Colloids and Surfaces A: Physicochemical and Engineering Aspects, 597, 124774.

Zhao, S., Pu, W., Wei, B. and Xu, X. 2019. A comprehensive investigation of polymer microspheres (PMs) migration in porous media: EOR implication. Fuel, 235, 249-258.

Zhao, T., Xing, J., Dong, Z., Tang, Y. and Pu, W. 2015. Synthesis of polyacrylamide with superb salt-thickening performance. Industrial & Engineering Chemistry Research, 54, 10568-10574.

Zhong, C., Yang, M. and Changchun, W. 2016. Viscous and Interfacial Behaviors, and AFM Morphologies of a Tetra-Polymer in Aqueous Solutions for Enhanced Oil Recovery. Chemical Engineering Communications, 203, 890-900.